A melting model for variably depleted and enriched lherzolite in the plagioclase and spinel stability fields

Christy B. Till,[1,2] Timothy L. Grove,[1] and Michael J. Krawczynski[1,3]

Received 18 November 2011; revised 24 April 2012; accepted 28 April 2012; published 20 June 2012.

[1] Here we develop a lherzolite melting model and explore the effects of variations in mantle composition, pressure, temperature, and H_2O content on melt composition. New experiments and a compilation of experimental liquids saturated with all of the mantle minerals (olivine, orthopyroxene, clinopyroxene, plagioclase and/or spinel) are used to calibrate a model that predicts the temperature and major element composition of a broad spectrum of primary basalt types produced under anhydrous to low H_2O-content conditions at upper mantle pressures. The model can also be used to calculate the temperature and pressure at which primary magmas were produced in the mantle, as well as to model both near-fractional adiabatic decompression and batch melting. Our experimental compilation locates the pressure interval of the plagioclase to spinel transition on the solidus and shows that it is narrow (~0.1 GPa) for melting of natural peridotite compositions. The multiple saturation boundaries determined by our model provide a method for assessing the appropriate mineral assemblage, as well as the extent of the fractional crystallization correction required to return a relatively primitive liquid to equilibrium with the mantle source. We demonstrate that an inaccurate fractionation correction can overestimate temperature and depths of melting by hundreds of degrees and tens of kilometers, respectively. This model is particularly well suited to examining the temperature and pressure of origin for intraplate basaltic volcanism and is used to examine the petrogenesis of a suite of Holocene basaltic lavas from Diamond Crater in Oregon's High Lava Plains (HLP).

Citation: Till, C. B., T. L. Grove, and M. J. Krawczynski (2012), A melting model for variably depleted and enriched lherzolite in the plagioclase and spinel stability fields, *J. Geophys. Res.*, *117*, B06206, doi:10.1029/2011JB009044.

1. Introduction

[2] The compositions of primitive basaltic magmas provide the principal evidence for interpreting the depth, temperature and style of melt generation in the Earth's upper mantle. Previous work has demonstrated near-fractional adiabatic decompression melting is the dominant process that forms mid-ocean ridge basalts (MORB) [*Klein and Langmuir*, 1987, 1989; *Kinzler and Grove*, 1992b; *Niu and Batiza*, 1991] and a number of major element mantle melting models have brought us closer to a rigorous quantitative description of this melting process [e.g., *McKenzie and Bickle*, 1988; *Kinzler and Grove*, 1992a, 1992b; *Langmuir et al.*, 1992; *Kinzler*, 1997]. An additional important but little explored factor is the effect of variations in the composition of mantle lherzolite on the derivative mantle melts. A significant portion of primitive basalts not erupted at MOR's, including many that form in continental back arc settings and at ocean islands, exhibit a greater range of K_2O (up to 2.0 wt.%), and P_2O_5 (up to 0.50 wt.%) relative to MORB, which is thought to be primarily the result of melting of compositionally variable lherzolite that has experienced different amounts of depletion and/or metasomatic enrichment. Furthermore, petrologic and geophysical constraints show that melting beneath the thick crust of continental margins and interiors may occur under near-batch melting conditions [*Bartels et al.*, 1991; *Holbig and Grove*, 2008]. Here we seek to examine lherzolite melting behavior over a wide range of upper mantle compositions applicable to the origin of basaltic lavas erupted in intraplate settings and develop a mantle melting model that explicitly takes into account the effects of variations in K_2O on mantle melting equilibria. The resulting model of lherzolite melting can identify the pressure and temperature of last equilibration with the mantle for a primitive basaltic magma, or be used in a forward model of melting lherzolite with a specific bulk composition. The latter application can provide useful information on the compositional characteristics of the mantle residue and the processes that produce melt with a given set of compositional characteristics. The magma composition derived by forward modeling can also be compared to the fractionation-corrected primitive basalt composition to

[1]Department of Earth, Atmospheric and Planetary Sciences, Massachusetts Institute of Technology, Cambridge, Massachusetts, USA.
[2]Now at U.S. Geological Survey, Menlo Park, California, USA.
[3]Now at Case Western Reserve University, Cleveland, Ohio, USA.

Corresponding author: C. B. Till, United States Geological Survey, Menlo Park, CA 94025, USA. (cbtill@usgs.gov)

0148-0227/12/2011JB009044

Table 1. Experiments Used in Our Plagioclase and Spinel Lherzolite Melting Model Calibration[a]

Reference	Number of Glasses Used	Starting Materials
Plagioclase Lherzolite		
This Study[b]	3	high K2O basalt, Jordan Valley OR, synthesized from oxides
Baker et al. [1994][b]	1	basalts, basaltic andesites, andesites, Mt. Shasta, CA
Bartels et al. [1991][b]	2	high alumina basalts, Medicine Lake, CA
Dunn and Sen [1994]	1	basalt and basaltic andesite, Mt. Adams, Washington
Falloon et al. [1997]	4	peridotite and corresponding low degree melts synthesized from oxides
Grove and Juster [1989][b]	10	basaltic andesite, Medicine Lake, CA and seeds of natural minerals
Kinzler and Grove [1992a][b]	10	MORB, natural samples and synthetic oxide mixtures
Presnall et al. [1979][b]	2	CMAS synthesized from oxides
Walter and Presnall [1994][b]	11	CMASN synthesized from oxides
Kushiro [1996]	1	Thaba Putsoa garnet lherzolite xenolith from Lesotho
	Total: 45	
Spinel Lherzolite		
Baker and Stolper [1994]	5	peridotite and corresponding low degree melts synthesized from oxides
Bartels et al. [1991][b]	3	see above
Falloon et al. [2001]	1	peridotite and corresponding low degree melts synthesized from oxides
Falloon et al. [1997]	2	see above
Gaetani and Grove [1998][b]	5	basalts, Medicine Lake, CA + synthetic oxide peridotite
Holbig and Grove [2008][b]	1	shoshonite, Tibet
Kinzler [1997][b]	26	peridotite synthesized from oxides
Kinzler and Grove [1992a][b]	14	see above
Kushiro [1996]	3	see above
Laporte et al. [2004]	14	depleted peridotite synthesized from minerals from a spinel harzburgite, Kane Fracture Zone
Pichavant et al. [2002]	1	high-MgO basalt, Soufriere, St. Vincent
Pickering-Witter and Johnston [2000]	8	peridotite synthesized from minerals from Kilbourne Hole, Hawaii
Presnall et al. [1979][b]	4	see above
Robinson et al. [1998]	8	peridotite or pyrolite and corresponding low degree melts synthesized from oxides
Villiger et al. [2004]	1	tholeiitic basalt, synthetized from oxides and seeds of natural minerals
Walter and Presnall [1994][b]	19	see above
Wasylenki et al. [2003]	8	peridotite synthesized from minerals from Kilbourne Hole, Hawaii + synthetic diopside
	Total: 123	

[a]All experiments from the studies listed, with the exception of those indicated in section 2.1, were used to calibrate the barometers and mineral component equations presented in Table 5.

[b]Experiments analyzed on the microprobe at MIT or performed on CMAS or CMASN bulk compositions, which were used to calibrate the thermometers in Table 5.

determine if the fractional crystallization correction was performed accurately.

[3] The mineral assemblage fractionally crystallized from a primary basaltic liquid en route to the Earth's surface has been shown to be the dominant control on the chemical variation of mid-ocean ridge basalts [*Walker et al.*, 1979; *Grove et al.*, 1992; *Langmuir et al.*, 1992; *Yang et al.*, 1996]. We examine the effect of different fractionating crystal assemblages and proportions on estimates of the temperature and pressure of MORB and ocean island basalt (OIB) generation from our model, as well as other thermometers and barometers. A worked example of the dual use of our model (i.e., forward model of lherzolite melting compared to thermobarometric calculations for a known basaltic liquid) is provided for a suite of primitive basaltic lavas erupted in the Diamond Crater area of Oregon's High Lava Plains (HLP).

2. Experimental Data

2.1. Experimental Data From the Literature

[4] A query was conducted in the Library of Experimental Phase Relations (LEPR) database [*Hirschmann et al.*, 2008] for experiments containing all of the five pertinent phases in lherzolite melting: glass, olivine, orthopyroxene, clinopyroxene, and plagioclase or spinel. Starting compositions of these experiments range from synthetic analogs of fertile or depleted mantle to natural MORB and high alumina olivine tholeiite (HAOT) lava samples (Table 1). The experiments returned by our query were divided into two categories: one for the plagioclase-bearing experiments, the other for spinel-bearing experiments (Table 1). Experiments that contained both plagioclase and spinel were included in both categories for model development. In addition to the experiments downloaded from LEPR, we added to our data sets fertile and depleted peridotite melting experiments from *Robinson et al.* [1998], spinel and plagioclase lherzolite melting experiments from an electronic supplement to *Kinzler* [1997], partial melting experiments on the Thaba Putsoa kimberlite by *Kushiro* [1996], peridotite melting experiments using diamond aggregate melt traps by *Baker et al.* [1995] and *Baker and Stolper* [1994], 0.1 MPa experiments from *Grove and Juster* [1989], CaO-MgO-Al_2O_3-SiO_2 (CMAS) experiments from *Presnall et al.* [1979], and CMAS+Na_2O (CMASN) experiments from *Walter and Presnall* [1994]. We used several criteria to evaluate the experimental liquid data set before modeling. First, experiments saturated with garnet were removed from the data set. Second, experiments conducted in the presence of water were also removed from the main data set and set aside for separate evaluation. Third, melts saturated with

Table 2. Composition of Experimental Starting Materials for Experiments Conducted in This Study

	JC-30B	Kragero Opx	JC-30B + 15% OPX	SpLM + OPX
SiO_2	48.92	57.3	50.18	48.11
TiO_2	1.74	0.06	1.49	0.92
Al_2O_3	16.13	0.1	13.73	15.12
Cr_2O_3	0	0	0	0
FeO	9.39	9.49	9.41	8.52
MnO	0.15	0.14	0.15	0.01
MgO	9.22	33.5	12.86	14.71
CaO	9.95	0.26	8.5	9.78
Na_2O	3.1	0	2.64	2.16
K_2O	0.97	0	0.82	0.59
P_2O_5	0.43	0	0.37	0.2
Mg#	0.64	0.86	0.71	0.75

olivine + orthopyroxene + clinopyroxene + plagioclase and/or spinel fall on generally consistent surfaces, referred to as multiple saturation surfaces, in pressure, temperature and composition space. We removed experiments that contain liquids that were clear outliers from the surfaces defined by the bulk of the data and ultimately >3σ from the model regression. These experiments include experiment #64 from *Takagi et al.* [2005], experiments #INT-A1, INT-A3, INT-D5, and INT-E7 from *Schwab and Johnston* [2001], experiment #L92 from *Kinzler* [1997], experiment #504 from *Kushiro* [1996], experiments 69a and 70a from *Baker et al.* [1995], and experiments #A1125, B1125, A1150, B1150 from *Meen* [1990]. Experiment numbers are those used by the original study. Fourth, following the initial regression of the data set we compared the trend defined by all the experimental liquids from an individual study in calculated versus known mineral component space to the data set as a whole. Using this technique we found that the experimental liquids from the studies of *Schwab and Johnston* [2001], *Draper and Johnston* [1992], and *Baker et al.* [1995] each define a slope <1 in calculated versus experimental mineral component space, unlike the majority of the data. Therefore all of the liquids from these studies were removed prior to the final regression of the full data set presented in Table 5. The 45 plagioclase lherzolite and 123 spinel lherzolite experiments that passed these evaluation techniques were included in the regression presented in Table 5.

2.2. New Experiments

[5] New experiments were also undertaken as part of this study (Tables 2, 3, and 4) to determine the phase relations and compositions for a high K_2O basaltic liquid in equilibrium with both a plagioclase and spinel lherzolite mantle phase assemblage. To this aim three sets of experiments were conducted. The first set of experiments utilized a high K_2O basaltic lava composition from Jordan Valley Volcanic Field in eastern Oregon (JC-30B), which was saturated with olivine, clinopyroxene, and plagioclase between 0.8 and 1.4 GPa and 1250–1310°C but failed to crystallize orthopyroxene. A second set of experiments, conducted with a derivative of the original starting material (JC30B+opx), were multiply saturated with olivine, orthopyroxene, clinopyroxene and plagioclase between 0.8 and 1.0 GPa. The third set of experiments was conducted on a high K_2O basaltic composition (SpLM+OPX) saturated with a spinel lherzolite mantle composition at 1.7 GPa; this composition was calculated using our model equations from Table 5. The third starting composition was saturated with olivine, clinopyroxene, and spinel at 1310°C, 1.7 GPa, and orthopyroxene, clinopyroxene and spinel at 1325°C, 1.7 GPa. These two experimental liquids are compositionally very close to each other (Table 4) and were spaced at the minimum temperature of reproducibility in the piston cylinder device. They bracket the spinel lherzolite mantle melting reaction point within experimental uncertainty. We therefore infer low-extent melts of mantle with the third bulk composition are in equilibrium with all of the mantle phases between the temperatures of these two experiments at 1.7 GPa (~1315–1320°C). In this paper we report only the results of the second and third set of experiments as these experiments are incorporated in our model and yield insights relevant for understanding melts saturated with a complete upper mantle phase assemblage.

3. Experimental and Analytical Methods

3.1. Starting Material

[6] A primitive basaltic composition with 48.43 wt% SiO_2, 0.96 wt% K_2O and a Mg# of 0.64 (Mg# = MgO/(FeO+MgO), molar units) from Coffee Pot Crater in the Jordan Valley Volcanic Field in eastern Oregon was chosen as the first starting composition for our experiments (JC-30B; Table 2). A synthetic oxide mixture of this composition was prepared and homogenized in an automatic agate mortar and pestle for three hours. Fe was added as Fe_2O_3 powder. A pellet of the homogenized starting material was then prepared using polyvinyl alcohol as a binder and hung on a Pt loop for conditioning in a DelTech 1 atm gas mixing furnace, using a CO_2-H_2 gas mixture. The sample was held at 1000°C for 28 h at the quartz-magnetite-fayalite (QFM) buffer in the furnace to ensure the iron in the starting material was dominantly FeO and all absorbed H_2O was evaporated, following the methods of *Grove and Juster* [1989]. The

Table 3. Experimental Run Conditions and Phases Present for Experiments Conducted in This Study

					Phases					
Experiment	Starting Materials	P (kbars)	T (°C)	Duration (hrs)	ol	opx	cpx	plag	sp	glass
B1204	JC30B+opx	8	1270	13.3	x	x	x	x		x
B1205	JC30B+opx	10	1250	75.3	x	x	x	x		x
B1149	JC30B+opx	10	1270	10	x	x	x	x		x
B1201	JC30B+opx	14	1270	28.8		x	x			x
C452	SpLM+opx	17	1310	76	x		x		x	x
C458	SpLM+opx	17	1325	77		x	x		x	x
C457	SpLM+opx	17	1340	48		x	x			x

Table 4. Normalized Major Element Composition of Experimental Phases From Our Experiments as Determined by Electron Microprobe Analysis[a]

Experiment	Phase	Number	SiO_2	TiO_2	Al_2O_3	Cr_2O_3	FeO	MnO	MgO	CaO	Na_2O	K_2O	NiO	P_2O_5	Total
							SpLM + OPX								
C452 (17 kbar, 1310C)	oliv	7	39.27	0.05	0.17		16.09		44.13	0.24			0.05		99.84
			0.33	0.02	0.02		0.53		0.26	0.03			0.05		
	cpx	15	50.55	0.61	11.1		5.72	0.02	17.1	13.62	1.27				99.8
			0.51	0.08	0.62		0.66	0.02	0.57	0.44	0.21				
	spinel	11	0.54	0.22	67.51		10.08	0.03	21.3	0.18			0.09		100.3
			0.23	0.03	0.72		0.57	0.03	0.29	0.03			0.13		
	glass	4	48.15	0.81	18.56	0.06	9.37	0.22	8.57	8.3	4.86	0.66	0.15	0.27	98.93
			0.26	0.07	0.16	0.06	0.45	0.17	0.67	0.29	0.54	0.01	0.15	0.06	
C458 (17 kbar, 1325C)	opx	5	51.71	0.43	10.93		8.73		24.28	2.86	0.95	0.11			100.17
			0.77	0.12	1.14		0.14		1.51	0.6	0.44	0.07			
	cpx	13	50.18	0.71	11.92	0.01	6.81	0.01	15.70	12.61	1.91	0.14			100.3
			0.55	0.10	1.19	0.01	0.41	0.01	1.48	1.05	0.65	0.12			
	spinel	7	0.54	0.22	67.56	0.03	10.92	0.02	20.49	0.17			0.01		100.5
			0.21	0.03	0.73	0.02	0.52	0.02	0.46	0.1			0.01		
	glass	6	48.83	1.30	18.61	0.01	9.52		7.46	7.13	6.01	0.72		0.40	99.69
			0.26	0.04	0.11	0.01	0.20		0.62	0.25	0.36	0.03		0.03	
C457 (17 kbar, 1340C)	opx	5	51.68	0.39	9.68	0.01	8.57	0.01	27.06	2.27	0.31	0.02			100.65
			0.8	0.05	0.83	0.01	0.22	0.01	0.31	0.33	0.15	0.02			
	cpx	5	50.1	0.66	11.38		6.69		18.00	12.08	1.07	0.02			100.36
			0.37	0.13	0.37		0.54		0.52	0.6	0.18	0.02			
	glass	4	48.53	1.17	19.04	0.02	8.85	0.01	8.27	8.18	4.81	0.71			100.48
			0.36	0.01	0.29	0.01	0.11	0.01	0.35	0.02	0.05	0.03			
							JC-30B + OPX								
B1204 (8 kbar, 1270C)	oliv	9	39.38	0.09	0.24	0.00	16.96	0.27	42.67	0.38			0.02		100.80
			0.61	0.02	0.23	0.01	0.49	0.02	0.77	0.16			0.03		
	cpx	7	51.36	1.13	5.74	0.00	6.34	0.19	18.58	16.17	0.54				100.96
			0.88	0.16	0.94	0.01	0.49	0.03	1.27	1.41	0.16				
	opx	5	52.41	0.60	8.48	0.00	10.37	0.21	23.81	3.42	0.67				99.96
			0.67	0.23	0.61	0.00	1.29	0.02	3.01	2.30	0.78				
	plag	11	53.97		25.70		2.21		1.51	10.62	4.94	0.46			100.41
			1.71		4.82		3.51		2.47	0.93	0.61	0.33			
	glass	10	51.62	1.98	17.27	0.02	8.90	0.16	6.24	8.77	4.03	1.01			100.87
			0.22	0.10	0.19	0.02	0.13	0.02	0.11	0.14	0.17	0.03			
B1205 (10 kbar, 1250C)	oliv	10	32.28	0.10	0.09	0.01	21.14	0.29	39.77	0.29			0.02		101.39
			0.19	0.01	0.01	0.01	0.29	0.02	0.51	0.03			0.02		
	cpx	17	51.27	0.99	6.34	0.04	7.66	0.22	17.57	15.32	0.58				100.80
			0.42	0.14	0.85	0.01	0.57	0.05	0.70	1.33	0.07				
	opx	3	53.03	0.78	7.15	0.00	10.05	0.21	23.72	4.22	0.83				99.83
			0.53	0.01	0.67	0.00	0.25	0.01	0.58	0.46	0.09				
	plag	9	54.79	28.51			0.34		0.13	10.82	5.10	0.31			100.00
			0.94	0.76			0.05		0.03	0.66	0.43	0.04			
	glass	9	50.17	2.61	17.38	0.00	10.40	0.18	5.48	7.09	5.39	1.30			99.95
			0.47	0.03	0.20	0.00	0.19	0.02	0.17	0.07	0.21	0.05			
B1201 (14 kbar, 1270C)	cpx	18	50.13	0.91	9.18	0.01	8.19	0.21	17.10	13.31	0.95				100.57
			0.67	0.14	0.78	0.01	0.34	0.03	0.68	0.67	0.15				
	opx	4	51.70	0.48	8.32	0.00	11.27	0.21	25.95	1.82	0.23				100.71
			0.41	0.06	0.38	0.00	0.10	0.03	0.46	0.08	0.08				
	glass	9	51.54	2.06	19.22	0.03	9.67	0.15	4.59	6.85	4.59	1.30			100.26
			0.32	0.03	0.23	0.03	0.12	0.01	0.41	0.15	0.17	0.06			
B1149 (10 kbar, 1270C)	oliv	5	38.48	0.07	0.11	0.01	19.17	0.19	41.60	0.36			0.01		99.72
			0.18	0.01	0.03	0.01	0.63	0.03	0.49	0.02			0.02		
	cpx	5	52.19	0.67	5.33	0.01	7.21	0.15	20.03	13.91	0.51				101.34
			0.18	0.06	0.51	0.01	0.19	0.02	0.32	0.35	0.04				
	opx	26	55.81	0.24	2.10	0.02	9.47	0.09	30.08	1.53	0.28				101.14
			1.87	0.27	2.89	0.01	0.40	0.08	3.98	1.75	0.47				
	plag	7	54.25	0.09	28.54	0.04	0.41	0.01	0.11	11.32	4.90	0.34			100.90
			0.30	0.01	0.18	0.02	0.02	0.01	0.01	0.22	0.13	0.01			
	glass	8	50.00	2.05	18.08	0.01	9.83	0.16	6.41	7.98	4.40	1.10			100.73
			0.39	0.16	0.18	0.01	0.28	0.02	0.12	0.04	0.26	0.05			

[a]The numbers in the second row of each entry represent the standard deviation based on replicate analyses. "Total" refers to the electron microprobe totals prior to normalization.

Table 5. Model Equations Produced by Multiple Linear Regression of Experimental Plagioclase and Spinel Lherzolite Liquids[a]

	Model Equations						r^2	Av. Abs. Error
Plagioclase Lherzolite								
T =	1216 +	104.4 (P) −	72.83 (1-Mg#) −	194.9 (NaK#) +	24.08 (TiO_2) −	1.55 (K_2O)	*0.95*	*11.70°C*
	9	*12*	*31*	*38*	*9*	*11*		
P = −	1.640 +	12.94 (Oliv) −	2.363 (1-Mg#) +	3.510 (NaK#) +	0.152 (TiO2) −	0.176 (K2O)	*0.95*	*0.08 GPa*
	0.130	*0.699*	*0.192*	*0.223*	*0.049*	*0.032*		
Oliv =	0.132 +	0.069 (P) +	0.173 (1-Mg#) −	0.261 (NaK#) −	0.009 (TiO_2) +	0.010 (K_2O)	*0.95*	*0.006*
	0.004	*0.004*	*0.014*	*0.014*	*0.004*	*0.003*		
Cpx =	0.238 −	0.051 (P) −	0.065 (1-Mg#) −	0.097 (NaK#) +	0.004 (TiO_2) −	0.013 (K_2O)	*0.81*	*0.012*
	0.008	*0.008*	*0.030*	*0.029*	*0.008*	*0.006*		
Plag =	0.408 +	0.146 (P) −	0.136 (1-Mg#) +	0.630 (NaK#) +	0.014 (TiO_2) −	0.028 (K_2O)	*0.98*	*0.012*
	0.008	*0.008*	*0.030*	*0.031*	*0.008*	*0.006*		
Qtz =	0.222 −	0.164 (P) −	0.029 (1-Mg#) −	0.272 (NaK#) −	0.009 (TiO_2) +	0.031 (K_2O)	*0.97*	*0.015*
	0.009	*0.008*	*0.033*	*0.033*	*0.008*	*0.006*		
Spinel Lherzolite								
T =	1212 +	119.9 (P) −	97.33 (1-Mg#) −	87.76 (NaK#) +	3.44 (TiO_2) −	4.58 (K_2O)	*0.96*	*10.78°C*
	8	*4*	*26*	*23*	*9*	*6*		
P = −	0.862 +	9.471 (Oliv) −	2.383 (1-Mg#) +	2.922 (NaK#) +	0.218 (TiO_2) −	0.146 (K_2O)	*0.85*	*0.15 GPa*
	0.12	*0.431*	*0.236*	*0.208*	*0.073*	*0.028*		
Oliv =	0.123 +	0.085 (P) +	0.203 (1-Mg#) −	0.268 (NaK#) −	0.019 (TiO_2) +	0.012 (K_2O)	*0.82*	*0.014*
	0.007	*0.004*	*0.024*	*0.021*	*0.007*	*0.003*		
Cpx =	0.180 +	0.005 (P) +	0.075 (1-Mg#) −	0.264 (NaK#) +	0.007 (TiO_2) +	0.012 (K_2O)	*0.4*	*0.025*
	0.012	*0.006*	*0.039*	*0.033*	*0.011*	*0.004*		
Plag =	0.554 −	0.043 (P) −	0.192 (1-Mg#) +	0.949 (NaK#) −	0.007 (TiO_2) −	0.041 (K_2O)	*0.89*	*0.025*
	0.012	*0.007*	*0.041*	*0.035*	*0.012*	*0.005*		
Qtz =	0.143 −	0.046 (P) −	0.085 (1-Mg#) −	0.416 (NaK#) +	0.020 (TiO_2) +	0.018 (K_2O)	*0.89*	*0.015*
	0.008	*0.004*	*0.026*	*0.023*	*0.008*	*0.003*		
Cpx Partition Coefficients *(P in kilobars)*								
D_{Na} = −	0.44 +	0.557 log(P)						
D_{Ti} =	22.57	$(P)^{-1.5}$						
Opx Partition Coefficients *(P in kilobars)*								
D_{Na} = −	0.15 +	0.166 log(P)						
D_{Ti} =	0.926	$(P)^{-0.56}$						

[a]Number in italics indicates the standard error for the coefficient above. For the model equations, temperature is in °C and pressure in GPa. Also presented are the pressure-dependent weight unit partition coefficient models for Na_2O and TiO_2 in orthopyroxene and clinopyroxene calculated using the experimental data incorporated in the model following the method of *Kinzler* [1997], where pressure is in kilobars.

QFM-conditioned starting material pellet was then reground into a powder with an automatic agate mortar and pestle. Because high pressure experiments on this composition failed to crystallize orthopyroxene on the liquidus, a second starting composition was subsequently fabricated using the original starting material and Kragero orthopyroxene (JC30B+opx; Table 2). Fifteen weight percent optically pure, hand-picked and crushed orthopyroxene was added to the original starting material and homogenized for three hours in the automatic agate mortar and pestle. A third starting material with 48.11 wt% SiO_2, 0.59 wt% K_2O and a Mg# of 0.75, which is a liquid composition calculated with our model to be in equilibrium with a spinel lherzolite at 1.7 GPa (SpLM+OPX; Table 2) was prepared following the methods described above for JC-30B. For each experiment, approximately 4 mg of the starting material was packed into a graphite capsule and held at ∼125°C for at least 24 h to ensure the experiments were conducted under nominally anhydrous conditions.

3.2. Piston Cylinder Experiments

[7] Experiments were performed in a 0.5″ end-loaded solid-medium piston cylinder apparatus [*Boyd and England*, 1960] in the MIT Experimental Petrology Laboratory using the setup detailed by *Médard et al.* [2008]. All experiments were conducted in graphite capsules ∼0.15″ in height. The capsules were placed in an Al_2O_3 sleeve, positioned in the center of a graphite furnace using MgO spacers, and encased in a sintered $BaCO_3$ pressure medium. The temperature was monitored and controlled using $W_{97}Re_3$-$W_{75}Re_{25}$ thermocouples positioned ∼1.5 mm above the capsule with no correction for the effect of pressure on thermocouple EMF. The experimental temperatures reported in Table 2 are corrected for the 18 ± 6°C offset in temperature between the thermocouple junction (colder) and the temperature of the sample located at the hot spot of the graphite furnace (hotter) [*Médard et al.*, 2008]. Pressure was calibrated using the breakdown reaction of Ca-tschermak pyroxene to anorthite + gehlenite + corundum (1350°C, 1.3 GPa) [*Hays*, 1966] and the spinel to garnet transition in the CMAS peridotite analog system (1500°C, 2.5 GPa) [*Hays*, 1966; *Longhi*, 2005] and no pressure correction was found to be necessary. The brackets achieved on these two phase transitions indicate that the run pressures are accurate to ±0.05 GPa. Experimental conditions are reported in Table 3.

3.3. Analytical Methods

[8] Major element concentrations of the experimental products were analyzed with the JEOL 733 or 8200 microprobes at Massachusetts Institute of Technology. All analyses of the individual phases presented in Table 3 were conducted with a 15 kV accelerating voltage, a 10 nA beam current and a beam diameter of 1 μm for crystalline phases and 10 μm for silicate glasses. Online data reduction used the CITZAF correction

package [*Armstrong*, 1995]. The analytical precision for glass analyses can be estimated from replicate analyses of a basalt glass working standard reported in *Gaetani and Grove* [1998]. Compositional variability for the experimental glasses reported in this study generally exceeds these values and thus represents compositional heterogeneity in the glass phase.

4. Experimental Results

[9] The compositions of the melts in equilibrium with plagioclase and spinel lherzolite from the previously published and new experiments are illustrated in Figure 1. At a given pressure, melts coexist with an upper mantle assemblage over a temperature range of ~50–150°C, which narrows toward higher pressures. The data set is well suited to explore the effects of oxides such as K_2O and TiO_2 on lherzolite melting as highlighted by the large variability in these oxides in the experimental liquids (~0–4 wt.% K_2O and ~0–2.75 wt.% TiO_2: Figure 1), especially in comparison to liquids produced in the CMAS system that plot at an Mg# of unity. The experimental liquids in these compositionally complex lherzolitic systems exhibit an overall covariation in NaK# ($(Na_2O+K_2O)/(Na_2O+K_2O+CaO)$), wt.% TiO_2, and wt.% Al_2O_3 with Mg#. Many of the plagioclase lherzolite experimental liquids are lower in Mg# than expected for melts in equilibrium with a mantle lherzolite bulk compositions (Mg# of liquid >0.72) (Figure 1). Experiments using natural basalts as starting materials do not saturate with the full spectrum of lherzolite phases until the liquids evolve to much lower Mg# than those expected to be in equilibrium with mantle residues. The inclusion of both these low Mg# liquids and liquids with Mg# = 1 from the CMAS(N) system aid in constraining the slopes of the parameters in the melting model and the overall fit of the models to the experimental data is very good. This is illustrated by the excellent parameter estimates for the plagioclase lherzolite model (Table 5) and indicate that the model will provide a robust approximation of liquids in the vicinity of Mg# = 0.7.

[10] The composition of the minerals and melts from our new experiments are given in Table 4. Three liquids in equilibrium with a plagioclase lherzolite assemblage have 1–1.3 wt.% K_2O and Mg#'s of 0.48–0.55. The two experimental liquids that bracket equilibrium with a spinel lherzolite assemblage at 1.7 GPa have 0.66–0.72 wt.% K_2O and Mg#s of 0.58–0.62. These liquids are very similar in their oxide content to other plagioclase and spinel lherzolite liquids compiled from the literature (Figure 1).

5. Parameterization of Plagioclase and Spinel Lherzolite Melting Equilibria

[11] Melting of plagioclase and spinel lherzolite is a five-phase equilibrium involving liquid + olivine + orthopyroxene + clinopyroxene + plagioclase or spinel. The thermodynamic variance of the melting equilibrium can be obtained from the Gibbs phase rule, $F = C + 2 - \phi$, where F is the number of degrees of freedom or variance, C is the number of components and ϕ is the number of phases [*Spear*, 1993]. In the CMAS system, these melting reactions have one degree of freedom and are univariant. Therefore, specifying the pressure of melting fixes the temperature and the composition of the melt. If an additional chemical component is added (e.g., Na_2O) [*Walter and Presnall*, 1994], the thermodynamic variance increases by one and the Gibbs method [*Spear*, 1993] can be applied to constrain the compositions of all coexisting phases. We choose to extend the univariant CMAS composition space into the natural system in our model by exploring the effects of additional compositional degrees of freedom on the melting equilibria, following *Longhi* [1991], *Grove and Juster* [1989], *Kinzler and Grove* [1992a], and *Kinzler* [1997]. The number of chemical components was chosen to be nine (this includes the dominant major and minor oxides required to calculate mineral components: SiO_2, TiO_2, Al_2O_3, FeO, MgO, CaO, Na_2O, K_2O, P_2O_5) and there are five mantle phases involved (olivine, orthopyroxene, clinopyroxene, plagioclase/spinel, melt), or six if plagioclase and spinel are both stable, therefore the thermodynamic variance of our system for plagioclase or spinel lherzolite is six, or five for plagioclase + spinel lherzolite. In previous studies, wt.% TiO_2, K_2O, Na_2O and Mg# have been identified as important compositional variables that systematically influence the composition of liquids in equilibrium with a lherzolite mineral assemblage [e.g., *Kushiro*, 1975; *Grove and Juster*, 1989; *Walter and Presnall*, 1994]. After extensive testing, we settled on an empirical model with four compositional variables in addition to pressure: 1-Mg#, NaK#, wt.% TiO_2, and wt.% K_2O (Table 5). Retaining only four compositional variables also allows a valid treatment of the variance of the 6-phase spinel + plagioclase lherzolite liquids in P-T-X space.

[12] An important variable that is neglected in this analysis is Cr_2O_3. The experimental data that constrain the spinel lherzolite melting reaction in this study all contain a high Al spinel and the amount of spinel consumed is small (~10–15% of the melting assemblage). As the melting extent increases, the Al content of the spinel phase continuously decreases. It is our sense that spinel eventually ceases to participate in the melting process as it becomes Cr-rich and the melting reaction thereby increases in variance. The Cr_2O_3 component of the melt is often not reported in this data set as a result of its low abundance. Therefore it is not possible for us to quantitatively evaluate the amount of Cr_2O_3-rich spinel involved in high-extent mantle melting reactions with the existing experimental data.

[13] We chose to express the composition of the spinel and plagioclase lherzolite melts in the model using mineral components in per-oxygen units because the mineral component values for experimental liquids vary systematically from their CMAS univariant values in response to changes in solid-solution exchange vectors like Mg-Fe and Ca-Na. We used the same pseudo-quaternary mineral component choice as *Kinzler and Grove* [1992a]: Olivine (Oliv), Clinopyroxene (Cpx), Plagioclase (Plag) and Quartz (Qtz). We converted the experimental liquid compositions from wt.% oxides to mineral components using the method of *Tormey et al.* [1987] with the correction of *Grove* [1993]. In addition, we calculated the two compositional parameters 1-Mg# (molar units) and NaK# (wt.% units, see Table 5) for each liquid. We then performed a least squares linear regression analysis using all of the experimental liquid compositions to produce three types of equations. The first is a thermometer with the four compositional parameters and pressure (in GPa) as the independent variables. The

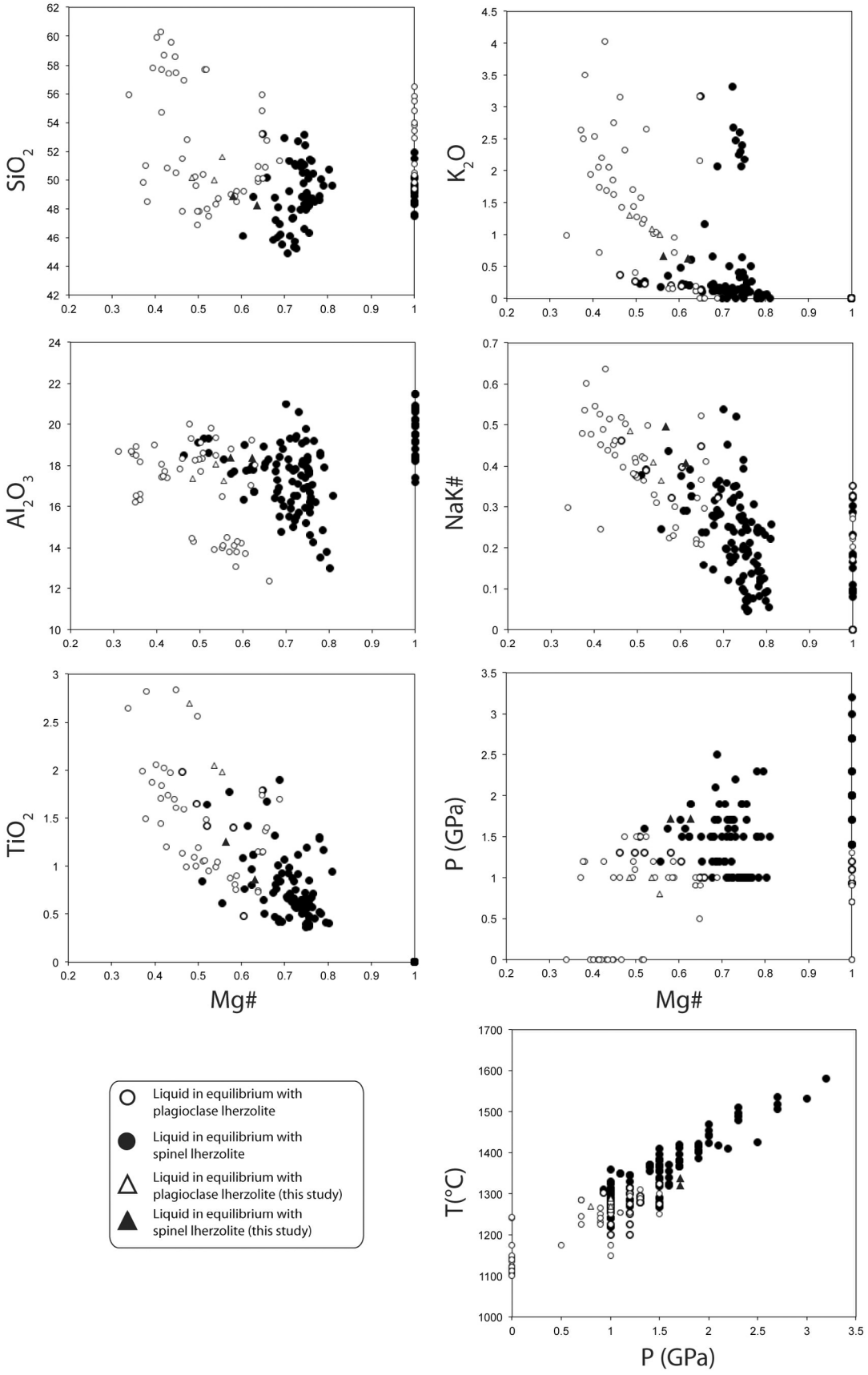
SiO2
K2O
Al2O3
NaK#
TiO2
P (GPa)
Mg#
Mg#
T(°C)
P (GPa)
Liquid in equilibrium with plagioclase lherzolite
Liquid in equilibrium with spinel lherzolite
Liquid in equilibrium with plagioclase lherzolite (this study)
Liquid in equilibrium with spinel lherzolite (this study)

Figure 1

second is a barometer with the olivine mineral component and the four compositional parameters as independent variables. The third type is a system of four equations that define the plagioclase and spinel lherzolite multiple saturation boundaries in the pseudo-quarternary space, utilizing the four compositional parameters and pressure (in GPa) as the independent variables. These equations are presented in Table 5 with one set of six equations for plagioclase lherzolite and another for spinel lherzolite. The standard error for the coefficients in each equation, as well as the coefficient of determination (r^2) and average absolute error (aae) for the entire equation are also presented in Table 5.

[14] The thermometer and barometer are designed to calculate the temperature and pressure of near primary mantle melts produced during melting of either plagioclase or spinel lherzolite. The system of four equations with mineral components as the dependent variables predicts the composition of plagioclase or spinel lherzolite saturated melts with variation in mantle pressure in pseudo-quaternary space. These four equations along with the thermometer reduce back to the univariant boundary in the CMAS system. In other words, when all four compositional parameters (NaK#, 1-Mg#, wt.% TiO_2 and K_2O) are zero as they are in the CMAS system, the temperature and the composition of a melt coexisting with olivine + orthopyroxene + clinopyroxene + plagioclase or spinel is constrained by pressure alone. As the bulk composition becomes more complex with the addition of other chemical components, the independent variables in these four equations other than pressure permit the prediction of a melt composition saturated with a lherzolite mineral assemblage. These equations are especially useful in modeling near fractional adiabatic decompression or batch melting of mantle with a known bulk composition as described in section 9. A worked example of how to linearly transform a melt composition expressed in per-oxygen mineral component units into oxide weight percent is presented in Appendix 1 of *Kinzler and Grove* [1992a].

[15] Plotted in Figure 2 are the observed values of the mineral components Oliv, Cpx, Plag and Qtz and the same value calculated using our equations from Table 5 for experimental liquids in equilibrium with spinel lherzolite, relative to a 1:1 line. The observed scatter in the calculated mineral component values in Figure 2 results from systematic differences in the pressure calibration and the electron microprobe standardization used to produce the experimental liquid compositions at different labs. For example, the synthetic peridotite melting experiments of *Kinzler and Grove* [1992a] and *Kinzler* [1997] were both analyzed using the same electron microprobe and standards at MIT but conducted at different piston cylinder labs. When the pressure of these experiments is calculated using our spinel lherzolite barometer equation, pressure is systematically overestimated for experiments conducted at the Lamont Doherty Earth Observatory (LDEO) experimental lab (Figure 3a), pointing toward a discrepancy in the pressure calibration between these two labs. An updated friction correction for high temperature experiments conducted in the LDEO lab [*Longhi*, 2005] resolves the discrepancy (Figure 3a). The pressures published for all experiments of *Kinzler* [1997] have therefore been corrected for use in the calibration of our model.

[16] The equations in Table 5 are qualitatively similar to the plagioclase and spinel lherzolite melting equilibria equations of *Kinzler and Grove* [1992a]. All the coefficients have the same sign and relative effect on the calculated temperature and the composition of the liquid expressed in mineral components with the exception of the pressure coefficient in the spinel lherzolite Cpx and Plag equations, which are very poorly resolved in *Kinzler and Grove* [1992a] and the 1-Mg# coefficient in the spinel lherzolite Qtz expression. The TiO_2 coefficient is better constrained in our equations relative to a majority of the *Kinzler and Grove* [1992a] equations where it is zero, although TiO_2 remains the variable with the largest errors relative to the magnitude of the coefficients in our equations. Our calculated 1 atm solidus temperature for the metastable spinel lherzolite assemblage is 55°C higher than that calculated by *Kinzler and Grove* [1992a] (Table 5), and our 1 atm plagioclase lherzolite solidus temperatures is 26°C lower than *Kinzler and Grove*'s [1992a]. In our equations, 1-Mg#, NaK# and K_2O lower the solidus temperature for both plagioclase and spinel lherzolite saturated liquids, and all other components serve to increase the solidus temperature. Pressure is positively correlated with temperature and the Oliv and Plag mineral components for a liquid in equilibrium plagioclase lherzolite, and temperature and the Oliv and Cpx mineral components for a liquid in equilibrium with a spinel lherzolite.

[17] The Cpx component exhibits the poorest fit to the experimental liquid data set, and has the least variability. Although melting of a lherzolite assemblage involves consuming a lot of clinopyroxene (i.e., the stoichiometric coefficient for cpx is the largest in the melting reaction) [*Kinzler and Grove*, 1999], the contribution from Cpx consumption does not vary significantly for the range of pressures and temperatures considered here. The low variability in the Cpx mineral component of the experimental liquids may be a result of the minimal change in the Cpx stoichiometric coefficient in the lherzolite melting reaction.

[18] The primitive liquid barometers (Table 5) were calibrated using the Oliv mineral component as an independent variable because this component reproduces the experimental pressures with the smallest average absolute error (0.08 and 0.15 GPa for plagioclase and spinel lherzolite, respectively) and has the best r^2 of the various mineral components. The primitive liquid thermometers in Table 5 were ultimately calibrated with only those experiments analyzed on the electron microprobe at MIT and experiments performed in the simple systems CMAS and CMASN. The majority of spinel lherzolite saturated experimental liquids not conducted in these simple compositional systems were produced at temperatures <1350°C and exhibit more scatter in the calculated temperature relative to the

Figure 1. Composition of the experimental liquids in equilibrium with a plagioclase (white circles) or spinel lherzolite (black circles) phase assemblage (olivine + cpx + opx ± plag ± spinel) modeled in our regression (see Table 1 for references). Experimental liquids produced as part of this study are shown as triangles.

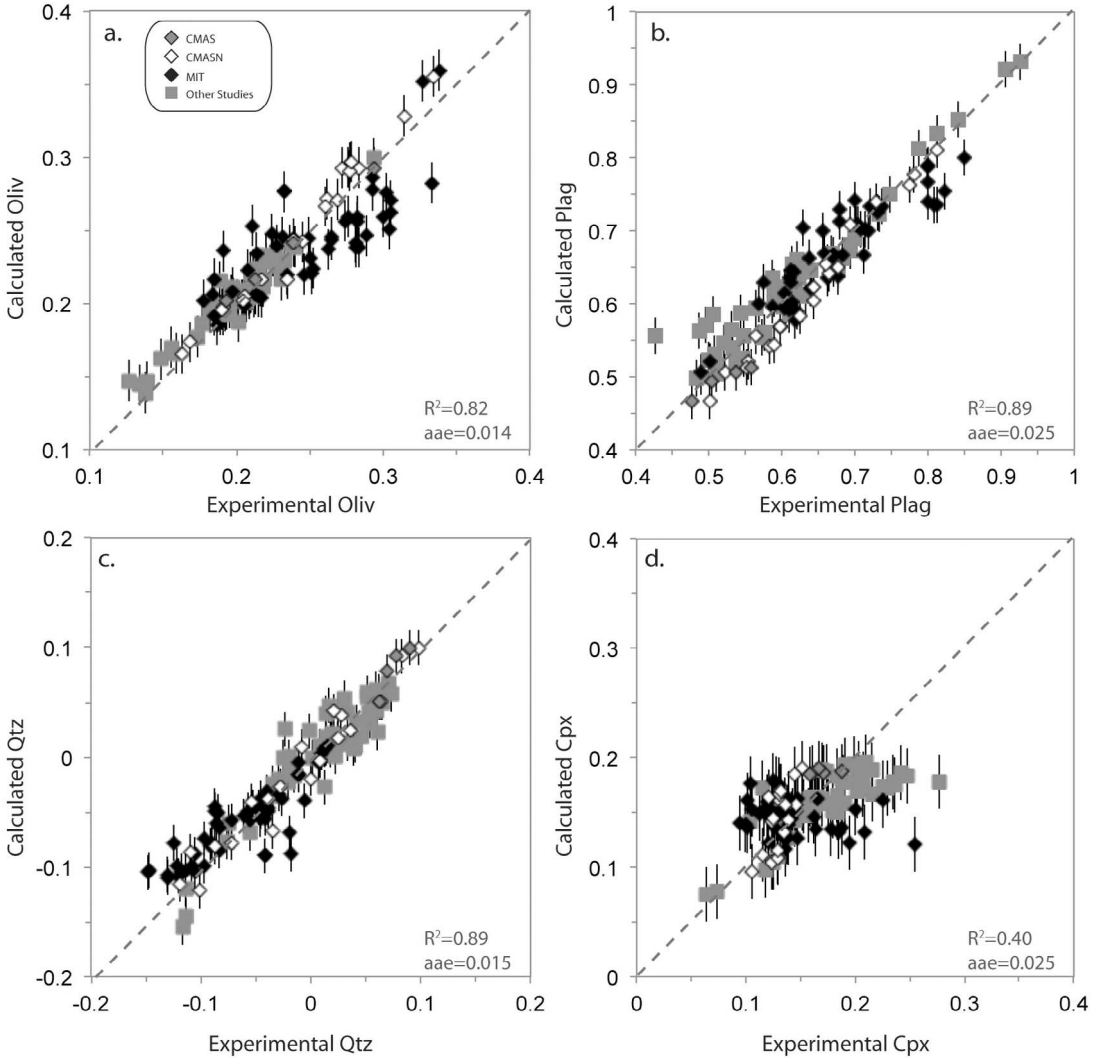

Figure 2. Experimental versus calculated mineral component values for the spinel lherzolite experimental liquids empirically fit by our regression. Dashed line represents 1:1 correspondence. Error bars correspond to the average absolute error (aae) produced by the mineral component equations in Table 5. The spinel lherzolite saturated experimental liquids are divided into the following four categories for comparison: (1) experiments conducted in the CMAS system (gray diamonds), (2) experiments performed in the CMASN system (white diamonds), (3) experiments analyzed on the electron microprobe at MIT (black diamonds), and (4) other experiments (gray squares). References for the experiments corresponding to each category can be found in Table 1.

CMAS(N) experiments. This scatter may be the result of differences in the temperature calibration between different experimental labs or the fact that the coefficient for 1-Mg# is very poorly resolved in the thermometer calibrated with the entire data set. The 1-Mg# coefficient is substantially better resolved for a regression of only the MIT analyzed and CMAS(N) experiments, which span the entire temperature range in the data set. The MIT + CMAS(N) calibrated plagioclase and spinel lherzolite thermometers have r^2 values of 0.95 and 0.96, respectively, and reproduce the experimental temperatures with average absolute errors that are equivalent to the temperature uncertainty of the experiments (~10°C). The plagioclase thermometer is calibrated over the temperature range of ~1100–1300°C and overlaps for ~50°C with the calibrated 1250–1550°C range of the spinel lherzolite thermometer. The overlap in these calibrations reflects the range of temperatures where both spinel and plagioclase are stable in the experimental data set.

6. Plagioclase Lherzolite to Spinel Lherzolite Boundary

[19] The compilation of experimental plagioclase and spinel lherzolite liquids allows us to revisit the location and primary controls on the plagioclase to spinel transition (PST) in the upper mantle. *Presnall et al.* [1979] locate the invariant PST in the CMAS system at 0.9 GPa and 1300°C. Additional experiments by *Walter and Presnall* [1994] in CMAS have both spinel and plagioclase present at 0.93 GPa,

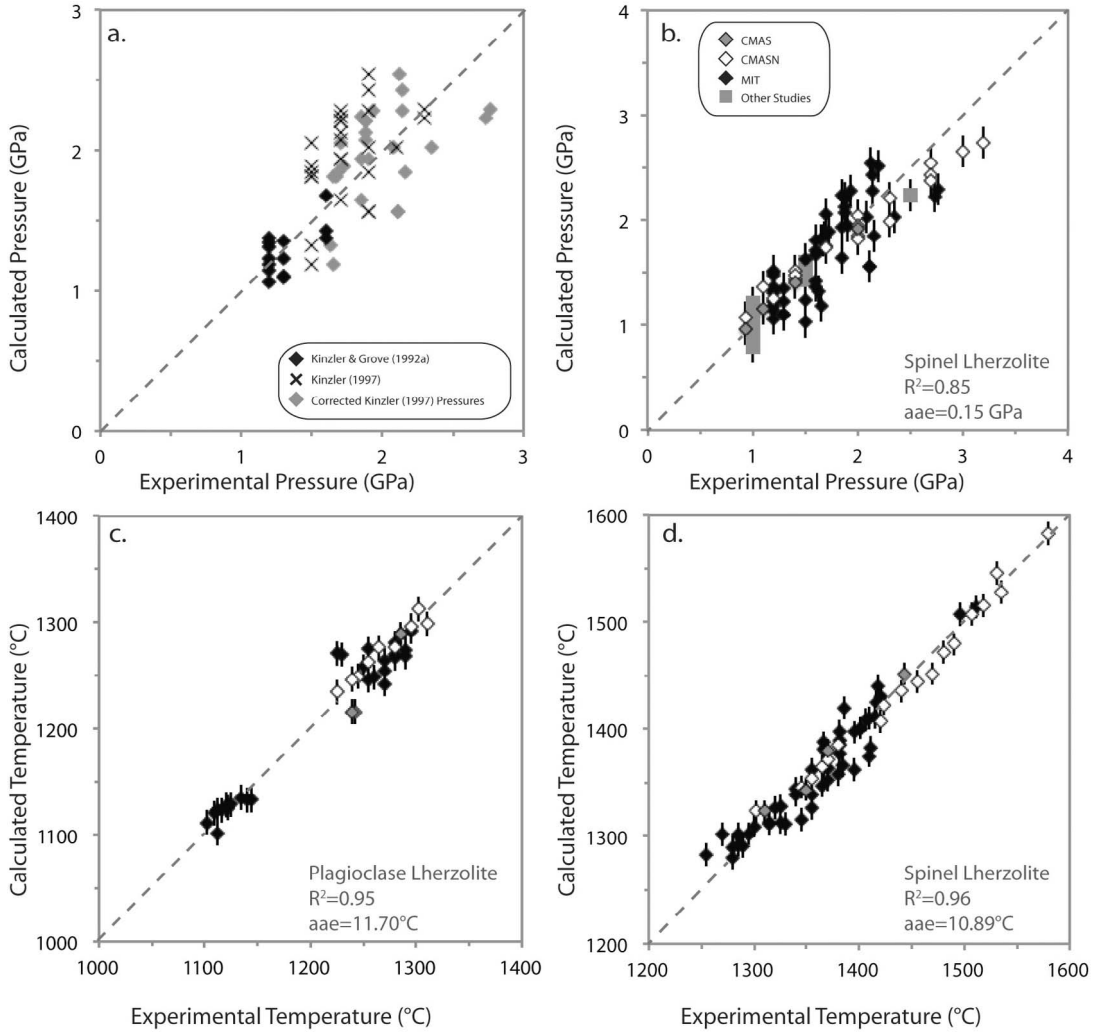

Figure 3. Experimental versus calculated pressures and temperatures for experimental lherzolite liquids. (a) Experimental versus calculated pressure for experiments from *Kinzler and Grove* [1992a] (black diamonds) and *Kinzler* [1997] (black crosses) using the spinel lherzolite barometer (Table 5). These two sets of experiments were conducted in different labs but analyzed on the same electron microprobe with the same standards, therefore the systematic differences in pressure between the two studies likely result from the inter-laboratory pressure calibration, not analytical differences. When the friction correction of *Longhi* [2005] is applied to the *Kinzler* [1997] experiments (gray diamonds), they produce a better fit to our barometer. (b) The experimental versus calculated pressure for the spinel lherzolite experimental liquids determined using the spinel lherzolite barometer in Table 5. Error bars correspond to the average absolute error (aae) determined from the experimental liquids used to calibrate the barometer. (c) The experimental versus calculated temperature for the plagioclase lherzolite experimental liquids determined with our plagioclase lherzolite thermometer in Table 5. (d) The experimental versus calculated temperature for the spinel lherzolite experimental liquids determined using the spinel lherzolite thermometer in Table 5.

with only plagioclase present at 0.7 GPa and only spinel at 1.1 GPa. *Kushiro and Yoder* [1966] found that the temperature-dependence of the PST was negligible. Experiments in the CMASN system [*Walter and Presnall*, 1994] show that there is a slight positive P-T slope to the univariant PST boundary and a strong NaK# dependence in *P*–(1-*NaK#*) space. In natural systems with more chemical variability, the data are too disparate and scattered in multicomponent space to add further insight on the P-T dependence of the PST. However, the NaK# dependence is well-defined by our experimental data set and an expression to define the NaK# dependence is

$$P = 1.56\,(\mathrm{NaK\#}) + 0.999 \quad (1)$$

where P is the pressure of the PST in GPa. This result reinforces earlier observations that the Na_2O/CaO content of the liquid, a proxy for the degree of depletion of the source, is positively correlated with the pressure of the PST [*Walter and Presnall*, 1994; *Falloon et al.*, 2008].

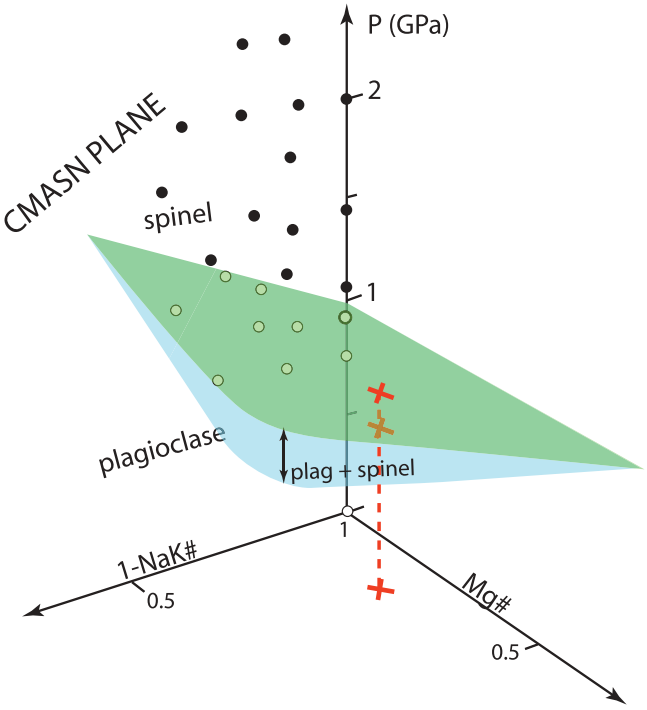

Figure 4. Illustration of the plagioclase-spinel lherzolite boundary in *Pressure-Mg#-(1-NaK#)* space. The plagioclase-spinel transition (PST) can be conceptualized as two bent screens (the plag-only to plag + spinel and plag + spinel to spinel-only boundaries) that define a three dimensional field with a height of ~0.3 GPa at high NaK#s and low Mg#s. This field collapses to a line in both the P-(1-NaK#) and P-Mg# planes. We plot 1-NaK#, rather than NaK#, to allow the CMASN experiments that constrain the slope of the univariant PST to be visualized on the plane where Mg# = 1. Also shown are experiments in the CMAS system that constrain the pressure of the PST at an Mg# and 1-NaK# of one. A typical upper mantle primitive liquid is illustrated by the red crosses.

[20] The PST expands from a univariant line in *P*–(1-*NaK#*) space into a divariant field in *P*–(1-*Nak#*)–*Mg#* space where both plagioclase and spinel are stable over a range of pressures and temperatures. This can be visualized in Figure 4 where the plagioclase→plagioclase+spinel and the plagioclase+spinel →spinel boundaries are depicted as two bent screens. Non-CMAS(N) experimental liquids that are in equilibrium with both spinel and plagioclase and have the highest NaK#'s and lowest Mg#'s in the data set suggest the maximum width of the PST field in *P*–(1-*Nak#*)–*Mg#* space is ~0.3 GPa. Therefore low extent mantle melts are in equilibrium with both plagioclase and an Al-rich spinel over a relatively narrow pressure interval. Typical mantle melts with an Mg# equal to 0.75 plot close to the Mg-axis, therefore plagioclase + Al-rich spinel are stable in these liquids over a pressure range much smaller (~0.1 GPa: 1.1–1.2 GPa) than 0.3 GPa. Metasomatic enrichment of mantle alkali contents will increase the NaK# of the mantle and slightly increase the pressure interval over which plagioclase and Al-rich spinel are stable.

[21] We can approximate the plagioclase + spinel→spinel boundary as a plane for practical use by using experiments both in the CMAS(N) and more complex compositional systems. Regression of experimental liquids on either side of the boundary yield the following expression for the pressure of this boundary in GPa:

$$P = 1.139(\text{NaK\#}) + 0.165(\text{Mg\#}) + 0.823 \quad (2)$$

An important shortcoming of this model is that it cannot deal with the presence of Cr-rich spinel found in natural depleted lherzolite [*Dick et al.*, 1984]. The key unresolved issue is how the Al-bearing component in spinel is partitioned between plagioclase and spinel at pressures lower than the PST transition. Cr-rich spinel is ubiquitous in natural depleted peridotite, but is extremely refractory and not likely involved in the lherzolite melting phase assemblage. For the purpose of this model we assume that the Al-spinel component reacts to form plagioclase and that an Al-spinel component ceases to participate in the melting reaction once the pressure interval of the narrow plagioclase + spinel transition has been traversed. It is assumed that a Cr-rich spinel remains as a residual phase in mantle lherzolite, and no longer takes part in the melting reaction at pressures in the plagioclase lherzolite stability field. Further experimental investigations are required to quantify the nature of participation of Cr-rich spinel in melting within the plagioclase stability field.

7. Implementation of the Plagioclase and Spinel Lherzolite Models

[22] Our lherzolite melting model can be used in two ways. The first is to estimate the depth and temperature of origin for a basaltic magma once it is corrected to remove the compositional effects of fractional crystallization. The second is to model mantle melting processes using specific lherzolite bulk compositions and melting styles (i.e., batch or fractional or in-between). The latter application can provide useful information on the compositional characteristics of the mantle residue and the processes that can lead to the production of a melt with a given set of characteristics. The composition derived in this second step can be compared to the fractionation-corrected composition to assess the accuracy of the fractional crystallization corrections. Ideally, all of these tasks should be carried out in a complimentary manner when one is trying to understand the origin of primitive basaltic magma.

7.1. Fractional Crystallization Corrections

[23] The first step in estimating the temperature and pressure of origin for primitive basalt is to correct for the effects of fractional crystallization that occurred between the source region and the Earth's surface. This step requires knowledge of the conditions under which the melt was modified by crystal fractionation, which in turn requires knowledge of the phase equilibria that control fractional crystallization under those conditions. The assumptions made in selecting the phase assemblage for the fractional crystallization correction can have a significant effect on the corrected liquid composition and therefore the estimates of source pressure and temperature, as evidenced by the comparison of the

thermometers and barometers for MORB compositions (see section 8). We illustrate the potential effects by discussing fractional crystallization for MORB, where the low-pressure fractional crystallization paths have been well established through experimental and petrologic studies [e.g., *Tormey et al.*, 1987; *Grove et al.*, 1992; *Yang et al.*, 1996]. For our fractionation corrections that involve only olivine and plagioclase, we used the methods of *Grove et al.* [1992] (see their Appendix 2). *Yang et al.* [1996] updated this method and we recommend using their approach if clinopyroxene is a fractionating phase. To choose the appropriate fractionating phase assemblage, the bulk sample compositions are plotted using oxygen units in the Olivine-Plagioclase-Clinopyroxene-Quartz pseudo-quaternary projection scheme of *Tormey et al.* [1987]. The location of the sample is compared to the location of the low-pressure saturation boundaries. For MORB these are the olivine – plagioclase – liquid (OPM) and the olivine – plagioclase – augite – liquid (OPAM) saturation boundaries. The proximity of the bulk composition to these boundaries dictates the initial fractionation assemblage that can be used to retrace the differentiation path. We use the method of *Grove et al.* [1992] updated with the plagioclase lherzolite multiple saturation point (MSP) recalibration presented here (Table 5) to calculate the MSP for the sample over a pressure range in the plagioclase stability field. As discussed in *Grove et al.* [1992] the location of this saturation boundary allows the position of the OPM and OPAM boundaries to be estimated over the crustal pressure range appropriate for the tectonic setting. By comparing the projected position of the sample to the projected position of the OPM and OPAM boundaries, the reverse fractional crystallization path may be traced to the point where the melt leaves the OPM boundary, enters the olivine primary phase volume, and follows an olivine-only addition path to one of the spinel lherzolite MSPs. This point is predicted for a near primary mantle melt saturated with olivine of a fixed composition (usually chosen as Fo_{90}) by calculating the melt components with the equations in Table 5 and the new Mg#, NaK#, and TiO_2 and K_2O content. If the melt is saturated with a plagioclase lherzolite assemblage, the OPM saturation boundary will coincide with the plagioclase lherzolite MSP and the olivine-only correction is not necessary. Experience in correcting near-primary basaltic liquids [*Gregg et al.*, 2009; *Elkins-Tanton et al.*, 2001] suggests that there is little ambiguity in reconstructing this path, because the OPM boundary crosses the spinel lherzolite MSP (Figure 5a) and the only possible olivine-only paths are dictated by these compositional constraints. The end product of this fractionation correction then places the MORB compositions at the appropriate MSP.

[24] This type of correction methodology is used to return the MORB glass compositions in section 8 (chosen from the

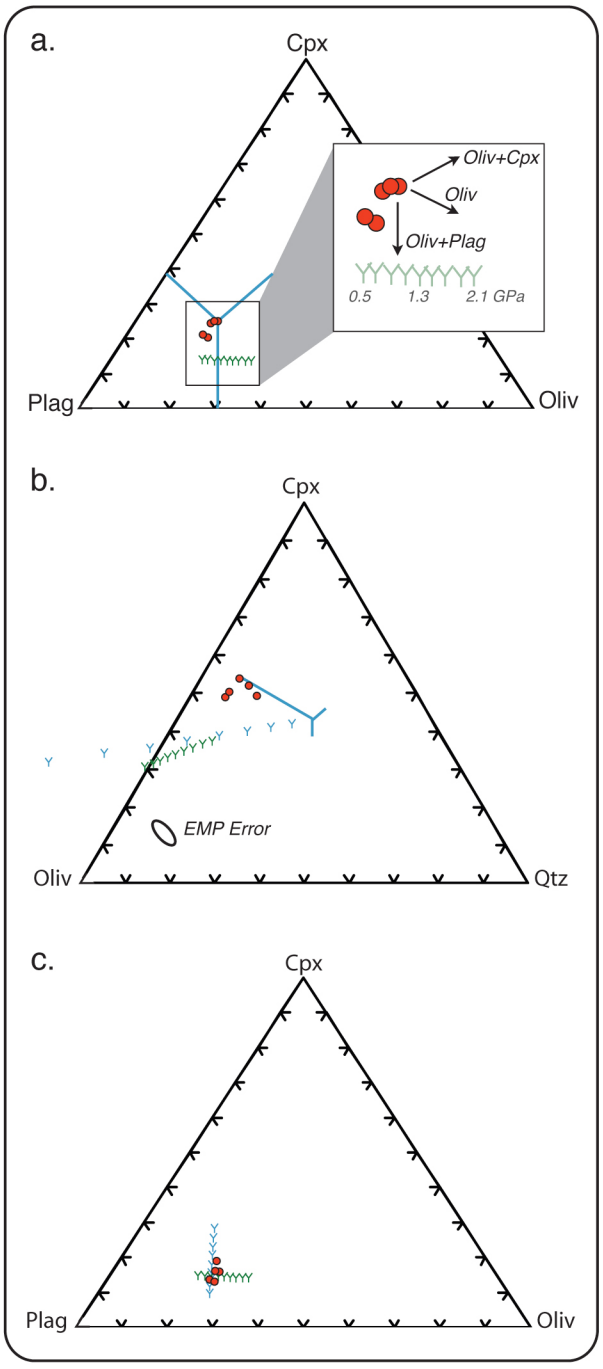

Figure 5. Rationale for fractional crystallization corrections depicted on pseudo-ternary projections. (a) Uncorrected average primitive glass compositions from the five MORB localities discussed in section 8 plotted with OPAM and OPM boundaries for 1 atm crystallization and the spinel lherzolite multiple saturation points calculated for the average Reykjanes MORB composition. Insert illustrates how different types of fractional crystallization corrections drive the glass compositions in very different directions relative to the spinel multiple saturation points. Gray numbers indicate pressures for the spinel multiple saturation points. (b) Uncorrected MORB compositions on Oliv-Cpx-Qtz pseudo-ternary plotted with OPAM and OPM boundaries for 1 atm crystallization and the spinel and plagioclase lherzolite multiple saturation points. The EPR and Azores average compositions lie on the OPAM boundary indicating 1 atm oliv+plag+cpx fractional crystallization for these liquids. (c) Average MORB glass compositions corrected for olivine and plagioclase crystallization using the methods described in section 5. Both plagioclase and spinel MSP are shown for a range of pressures from 1 atm to 2.1 GPa.

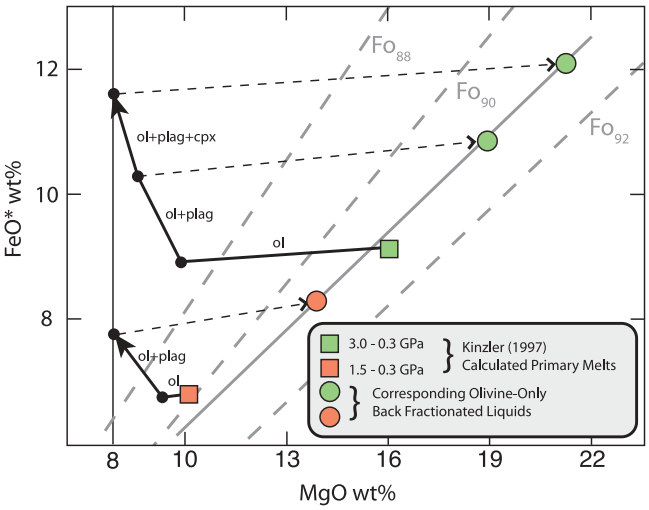

Figure 6. Effect of olivine-only reverse fractionation correction on mantle melts that experienced a multiphase fractionation history. Two calculated primary melts generated by polybaric, near fractional melting [*Kinzler*, 1997] are shown for 3.0–0.3 GPa and 1.5–0.3 melting models (green and orange squares). Also shown are calculated forward model fractional crystallization paths experienced by these primary melts at 0.1 MPa (solid lines showing the crystallizing assemblage). These forward model fractionation calculations were performed in a similar manner to those outlined in section 7.1, only in reverse. The fractionation paths (black lines and dots) shown for olivine, followed by olivine + plagioclase, and for the 3.0–0.3 GPa primary melt, a third period of olivine + plagioclase + clinopyroxene fractionation move the melts along saturation boundaries to 8 wt.% MgO. These melts now have the FeO_8 composition used as a starting point for MORB melting models [e.g., *Klein and Langmuir*, 1987; *Langmuir et al.*, 1992]. These fractionated melts are then corrected for olivine-only addition until they are in equilibrium with Fo90 olivine following the *Herzberg and Asimow* [2008] liquid composition-dependent K_D for olivine-melt (solid gray line). Also shown for comparison are contours of liquid compositions using a constant olivine-liquid Fe-Mg K_D of 0.3 (dashed gray lines). The resulting reverse fractionated liquids (green and orange circles) are considerably different from the original *Kinzler* [1997] calculated primary melts.

PetDB database) to near primary melts. The phase equilibria for MORB glasses of similar composition are well established and discussed for the global MORB data set in *Grove et al.* [1992]. The corrected compositions in Figure 5c required olivine + plagioclase fractionation, or in the case of the EPR and Azores compositions olivine + plagioclase + clinopyroxene and olivine + plagioclase fractionation. Only a small amount of olivine-only addition is required because these liquids are near a spinel lherzolite MSP that is very close to the OMP boundary.

[25] Here we emphasize that applying the appropriate fractionation correction (oliv; oliv + plag; oliv + cpx; or oliv + plag + cpx) is essential for returning a fractionated basalt composition to its mantle melt precursor. This calculation can be applied with confidence for MORB melts, because the phase relations are well known, but such a situation does not exist for all basalts. We illustrate the way in which changes in the mineral assemblage chosen for the correction might affect thermometric and barometric calculations for primitive basalts. Two polybaric, near-fractional aggregated MORB primary melts [from *Kinzler*, 1997], which span the range of melting conditions beneath global MOR systems, are used to illustrate this point in Figure 6. Also shown are the forward-modeled fractional crystallization paths at 0.1 MPa for these two primary magmas to 8 wt.% MgO as calculated by *Kinzler* [1997]. The two derivative liquids that have experienced multiphase fractionation are then arbitrarily corrected with a reverse fractional crystallization process where olivine is the only phase added. The reverse-fractionation process is performed until the liquid is in equilibrium with Fo90 olivine. The resulting fractionation-corrected liquids contain significantly higher FeO and MgO than the actual parental liquid. For the 8 wt.% MgO composition derived from the 1.5–0.3 GPa primary magma, olivine-only reverse fractionation produces a "corrected primary melt" that yields a temperature and pressure estimate from our model that is 104°C and 0.85 GPa higher than the actual average temperature and pressure of origin for the primary MORB liquid. When the same operation is performed for the 3.0–0.3 GPa liquids, the reverse fractionation process using only olivine yields temperature and pressure estimates for the "corrected primary melt" that are up to 158°C and 1.33 GPa higher than the original primary MORB liquid. Figure 6 also illustrates how the choice of olivine Fo-content for the mantle residue can have a significant effect on the FeO and MgO of the fractionation corrected liquid and thus any temperature and pressure calculations using that composition.

7.2. Effect of H_2O

[26] Three experimental studies [*Gaetani and Grove*, 1998; *Hirose and Kawamoto*, 1995; *Kushiro*, 1990] report the composition of H_2O-undersaturated melts in equilibrium with a complete spinel lherzolite mantle phase assemblage. These data can be used to constrain the effect of H_2O on the pressure and temperature of melting and thus develop an adjustment for the influence of H_2O on our spinel lherzolite thermometer and barometer. A similar data set does not exist to evaluate the influence of H_2O on our plagioclase lherzolite thermometer and barometer. When the temperature and pressure of the H_2O-undersaturated spinel lherzolite melting experiments are plotted against those predicted by our spinel lherzolite thermometer and barometer for the experimental liquid compositions, the experiments of *Gaetani and Grove* [1998] and *Hirose and Kawamoto* [1995] reveal a consistent trend regarding the influence of H_2O on melting conditions and melt compositions, while the experiments of *Kushiro* [1990] do not. Because the *Kushiro* [1990] experiments are sandwich experiments with very short durations (24 h), it is possible that the melt and the large volume of crystalline solids in the sandwich were not in equilibrium. Durations of >72 h are the preferred minimum time for sandwich experiments [*Falloon et al.*, 2001]. For these reasons we chose to exclude the experiments of *Kushiro* [1990] from our regression of the hydrous experimental data.

[27] The H_2O-undersaturated experiments demonstrate the effect of dissolved H_2O in a basaltic liquid is to decrease the

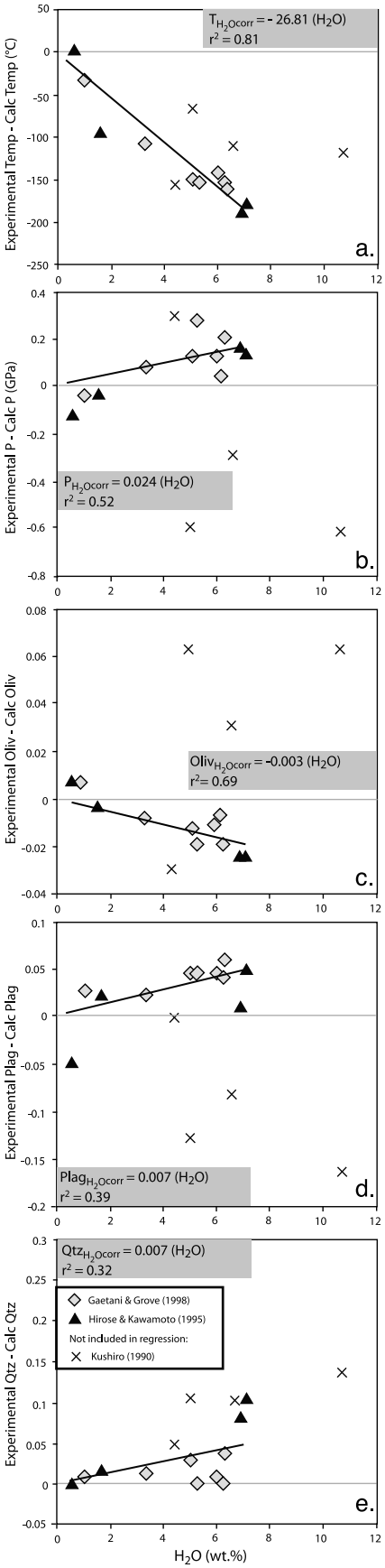

temperature and increase the pressure of mantle equilibration, consistent with previous studies on the effect of H_2O on mantle melting processes [e.g., *Kushiro et al.*, 1968; *Green*, 1973; *Grove et al.*, 2006]. The resulting correction for the effect of H_2O on temperature and pressure calculated using our spinel lherzolite thermometer and barometer is given in Figure 7. These corrections are considered applicable over the range of H_2O contents in the experiments used in the regression (0–7 wt.%). The corrections are designed to be applied after an initial estimate of the temperature and pressure of last mantle-melt equilibration for a given primitive basaltic melt are calculated using the expressions in Table 5 and where an estimate of the pre-eruptive H_2O-content of the basaltic melt can be determined from magma hygrometers [e.g., *Sisson and Grove*, 1993] or melt inclusions [e.g., *Hauri*, 2002].

[28] Although application of the H_2O correction term to our thermometer and barometer is relatively straightforward, the interpretation of the origin of H_2O-bearing magmas and the significance of the temperature, pressure, and melt composition estimates are more complicated. With anhydrous melting two end-member styles for mantle melting can be considered: fractional or batch melting. More complicated reactive porous flow models can also be imagined and these can be modeled using the methods discussed here with the additional complication of tracking the change in the mantle residue composition during melt-wall rock interaction. For the end-member example of fractional melting, where fractional melting increments are created over a range of pressures and accumulated, our thermometer and barometer produces estimates that represent the average pressure-temperature (P-T) conditions (for the entire melting column) at which a melt was in equilibrium with the mantle [*Asimow and Longhi*, 2004], and in the case of batch melting, the last P-T conditions at which a melt was in equilibrium with the mantle (see discussion of distinguishing between these two anhydrous melting processes in section 9). However, there are a variety of paths along which the mantle could evolve to end up at the P-T-H_2O conditions represented by the H_2O-

Figure 7. Effect of H_2O on our equations for calculating the temperature, pressure, and the olivine, plagioclase and quartz mineral components for a melt in equilibrium with spinel lherzolite. (a) Difference between the experimental temperature and the temperature calculated using the spinel lherzolite thermometer (Table 5) for experimental liquids from H_2O-undersaturated mantle melting experiments of *Hirose and Kawamoto* [1995] and *Gaetani and Grove* [1998]. The corresponding correction to our spinel lherzolite thermometer is shown in the gray box with H_2O in wt. %. (b) Difference between the experimental pressure and the pressure calculated for the H_2O-undersaturated experimental melts using the spinel lherzolite barometer. (c) Difference between the H_2O-undersaturated melt's Oliv component and the Oliv component calculated for the experimental melt using the spinel lherzolite Oliv equation. (d) Difference between the melt's Plag component and the Plag component calculated for the H_2O-undersaturated experimental melts using the spinel lherzolite Plag equation. (e) Difference between the melt's Qtz component and the Qtz component calculated for the H_2O-undersaturated experimental melts using the spinel lherzolite Qtz equation.

undersaturated melting experiments. For example, if there is sufficient H_2O present in the mantle to saturate the nominally anhydrous minerals olivine, orthopyroxene, clinopyroxene and the aluminous phase (i.e., 0.055 wt.% at 0.1 GPa to ~0.3 wt.% at 6 GPa) [*Hauri et al.*, 2006], the mantle will incipiently melt at the low temperature of the H_2O-saturated solidus [*Till et al.*, 2012] and if melting continues, the H_2O will become progressively diluted in the melt to end up at the P-T-H_2O conditions of the H_2O-undersaturated experiments. Alternatively, the mantle could contain enough H_2O and alkalis to stabilize a hydrous phase such as amphibole, which could trigger dehydration melting or when in contact with a melt percolating upward in the mantle, contribute H_2O to the pre-existing melt. Thus a myriad of paths exist along which a mantle melt could end up at a given set of P-T-H_2O conditions. These are beyond the scope of this paper but a variety of mantle melting processes could be tested using the expressions presented here (Table 5).

[29] Included in Figure 7 are corrections for the effect of H_2O on the spinel lherzolite Oliv, Plag and Qtz equations in Table 5. We do not include a correction for the Cpx component of the melt composition because it yields no consistent change with increasing H_2O content and the H_2O-bearing experimental liquids falls within the uncertainty for the equation calibrated with the anhydrous liquids (Table 5). This is likely because of the near constant value of the Cpx exhibited by all of the experimental liquids in the data set. The corrections to the Oliv, Plag and Qtz equations should be incorporated when the spinel lherzolite MSP presented in this paper are used for forward modeling of mantle melting at H_2O-undersaturated conditions as described below.

7.3. Calculating Melts of Mantle Lherzolites

[30] The forward model of plagioclase and spinel lherzolite melting we use here is an update of the model presented by *Kinzler and Grove* [1992a, 1992b] that incorporates the improvements of *Kinzler* [1997]. In order to use the melting model, the Mg# and abundances of minor components in each melt increment must be inferred. Estimates of the minor components are obtained using the non-modal batch melting equation:

$$C_i = C_o/(D_B + F(1 - P_B)) \quad (3)$$

where C_i is the concentration of the minor component (e.g., K_2O) in the melt, C_o is the concentration of that component in the bulk solid, D_B is the partition coefficient for the component between solid and melt, F is the extent of melting, and P_B is the bulk solid-melt partition coefficient for the component weighted by the stoichiometric coefficients in the melting reaction (wt.% units). Partition coefficients have been calculated using the experimental data that is incorporated in the model. The partition coefficient models for Na_2O and TiO_2 in orthopyroxene and clinopyroxene are pressure-dependent, following the method of *Kinzler* [1997]. These weight unit partition coefficients are found in Table 5. The remaining constant partition coefficients are from *Kinzler* [1997] but were recast into weight units.

[31] Our model uses the pressure-dependent spinel lherzolite melting reaction calibrated by *Kinzler* [1997] and the plagioclase lherzolite melting reaction of *Kinzler and Grove* [1992b]. The Mg# of a melt coexisting with a lherzolite composition is determined by solving equations for the conservation of mass for FeO and MgO between lherzolite and a given fraction of melt, following the method of *Kinzler and Grove* [1993]. These equations require knowledge of the partitioning of Fe and Mg between melt and all the coexisting phases, and the exchange K_D's for Fe and Mg are calculated from the experimental data set. The value for $K_D^{Fe\text{-}Mg}$ for olivine is known to vary with pressure and melt composition [*Ulmer*, 1989; *Toplis*, 2005]. We set the $K_D^{Fe\text{-}Mg}$ values for clinopyroxene, orthopyroxene and spinel to 0.94, 0.97 and 1.5 times the $K_D^{Fe\text{-}Mg}$ value for olivine-melt as discussed by *Kinzler and Grove* [1992b] and *Kinzler* [1997], allowing the compositional variations in $K_D^{Fe\text{-}Mg}$ to be applied to all phases.

[32] Melting in the model can be specified to be either batch or polybaric near-fractional adiabatic decompression melting and the melt production rate for polybaric melting can be varied depending on preference for the heat of fusion. We recommend a value of ~1 wt.% per 0.1 GPa of decompression at low extents of melting (≤~4–8 wt.%). For higher extents of melting the isentropic melt production rate cannot be modeled as linear [*Asimow et al.*, 1997]. In the case study presented in section 9, we use this forward model to test models of both batch and near-fractional upper mantle melting to generate basalts from Oregon's HLP.

8. Comparison of Parameterization to Other Thermometers and Barometers

[33] Previous major element models of upper mantle melting focus on the generation of MORB and by inference the MORB-source mantle [*Klein and Langmuir*, 1987; *McKenzie and Bickle*, 1988; *Niu and Batiza*, 1991; *Kinzler and Grove*, 1992a, 1992b; *Langmuir et al.*, 1992; *Kinzler*, 1997]; they do not consider melting of variably depleted and/or enriched lherzolite. Other thermometers, barometers and melting models aim to investigate the production of a wider range of basalt compositions (e.g., OIB) but are calibrated on experimental liquids that are in equilibrium with olivine only [e.g., *Ford et al.*, 1983; *Putirka*, 2005; *Putirka et al.*, 2007] or olivine + orthopyroxene only [*Lee et al.*, 2009]. To explore the differences that might arise in estimating melting conditions for basaltic liquids with a model calibrated exclusively on liquids saturated with the complete upper mantle phase assemblage of olivine + orthopyroxene + clinopyroxene + plagioclase and/or spinel, we compare our thermometric and barometric estimates for five different locations of MORB genesis and three locations of OIB genesis to those from a variety of extant mantle thermometers and barometers.

[34] MORB compositions were compiled from PetDB ocean rock database using the latitude and longitude of the selected areas, filtered for fresh glass analyses (MgO > 8 wt.%) and averaged before they were corrected for olivine-only and alternatively olivine + plagioclase fractionation until they were in equilibrium with a Fo90 mantle olivine following the methods described in section 7.1 (Table 6). Pressure estimates are required for the thermometers of *Ford et al.* [1983], *Kinzler and Grove* [1992a], *Langmuir et al.* [1992], *Putirka et al.* [2007] and the thermometer presented here (Table 5), and were calculated for the fractional crystallization

Table 6. MORB Glass Analyses (MgO > 8 wt.%) From the PetDB Data Base Corrected for Olivine + Plagioclase Fractionation Until They Were in Equilibrium With a Fo90 Mantle Olivine Following the Methods Described in Section 7[a]

	SiO_2	TiO_2	Al_2O_3	Cr_2O_3	FeO	MnO	MgO	CaO	Na_2O	K_2O	P_2O_5	Total
Reykjanes	48.84	0.74	17.60	0.00	7.58	0.00	11.49	12.03	1.68	0.05	0.00	100.00
SWIR	48.42	1.03	18.07	0.00	7.68	0.00	11.45	10.98	2.29	0.08	0.00	100.00
EPR 9N	48.41	0.85	17.83	0.00	7.54	0.00	11.28	12.12	1.91	0.06	0.00	100.00
Kane FZ	48.97	1.01	17.99	0.00	7.34	0.00	11.13	11.09	2.40	0.08	0.00	100.00
Azores	49.56	0.90	17.05	0.00	7.28		10.98	12.16	1.89	0.19	0.00	100.00

	This Study Melt Comp. Calc								*Lee et al.* [2009]	
	Qtz	Plag	Oliv	Cpx	Mg#	NaK#	P Calc	T Calc	P Calc	T Calc
Reykjanes	0.044	0.578	0.226	0.152	0.73	0.13	1.16	1316	0.68	1325
SWIR	0.019	0.622	0.235	0.123	0.73	0.18	1.44	1346	0.80	1326
EPR 9N	0.025	0.597	0.219	0.159	0.73	0.14	1.15	1314	0.90	1323
Kane FZ	0.022	0.624	0.222	0.133	0.73	0.18	1.34	1333	0.74	1314
Azores	0.041	0.573	0.205	0.180	0.73	0.15	1.03	1299	0.68	1309

[a]The corresponding pressure and temperature estimates for these corrected liquids were made with our spinel lherzolite thermometer and barometer (Table 5) and the *Lee et al.* [2009] thermometer and barometer.

corrected compositions at each location using the barometers of *Lee et al.* [2009] and the spinel lherzolite barometer from this study (Table 5). In the case of MORBs, which are polybaric near-fractional melts [*Johnson et al.*, 1990], the calculated pressure represents an average pressure for the entire melting column [*Asimow and Longhi*, 2004]. Our barometric estimates for the olivine+plagioclase corrected MORB compositions are 0.25–0.64 GPa greater than those estimated with the *Lee et al.* [2009] barometer (Table 6). However, our pressure estimates for the olivine + plagioclase corrected MORB compositions are within 0.16 GPa of the pressures estimated by *Lee et al.* [2009] for the olivine-only corrected MORB compositions and both are within the range of accepted values for MORB generation [*Kinzler and Grove*, 1992b] (Figure 8e). Our pressure estimates for the olivine-only corrected compositions are quite high relative to average MORB generation pressures, because our barometer is sensitive to the increase of 0.02–0.04 in NaK# and 0.02–0.03 in Mg# for the olivine-only corrected liquid relative to the olivine + plagioclase corrected liquid. The temperature estimates for each location vary up to 185°C between thermometers when calculated with olivine-only corrected compositions (Figure 8a) or 117°C when calculated with the olivine + plagioclase corrected compositions. It is interesting to note that all temperatures for the MORB localities cluster around 1300°C when the olivine + plagioclase corrected compositions are used with the exception of the *Ford et al.* [1983] thermometer (Figure 8b). This suggests the variety of methods employed by the different thermometers compared here are all proportionally sensitive to the chemical variability of the liquid produced by different types of crystal fractionation corrections. It also appears that when corrected for crystal fractionation using the constraints from our low-pressure fractionation model (section 7), the various thermometers converge on similar source temperature estimates. This comparison of thermometers also reveals that calculations of mantle temperature for MORB depend on the type of fractionation correction, in addition to the source pressure.

[35] Determining the temperature and pressure for OIB genesis is significantly more complicated due to the paucity of primitive OIB that can be positively identified as liquids and the abundance of compositions that have experienced complex fractional crystallization and other pre-eruptive processes after they segregated from a peridotitic source. Glasses from Kilauea volcano in Hawaii represent some of the only picritic glasses from a hot spot locality and work by *Wagner and Grove* [1998] reveals these liquids were never in equilibrium with garnet lherzolite assemblage on their liquidus. Rather, these tholeiites appear to have been in equilibrium with a harzburgitic source at lithospheric depths. Studies of Kilauea tholeiites by *Wagner and Grove* [1998] and Mauna Kea submarine glasses by *Stolper et al.* [2004] suggest they formed by melting of garnet lherzolite in a mantle plume, followed by equilibration of the liquids with a harzburgitic mantle at shallow depths. In addition, many primitive OIBs, such as those from Samoa [*Workman et al.*, 2004], Marquesas [*Desonie et al.*, 1993] and the Ontong Java plateau [*Herzberg et al.*, 2007], exhibit evidence for olivine and/or clinopyroxene accumulation. Therefore reconstructing the parental liquid composition of an OIB in order to calculate the source pressure and temperature is not simply a matter of determining the right phase assemblage for the fractionation assemblage, as is the case for MORB. A number of techniques have been developed to circumvent these issues and calculate the parental liquid for a given OIB compositions [e.g., *Putirka et al.*, 2007; *Herzberg and Asimow*, 2008]. Parental liquid compositions for selected OIBs calculated by *Putirka et al.* [2007] plot in a location on a series of pseudo-ternary projections that are not consistent with liquids in equilibrium with plagioclase or spinel lherzolite as determined by our model, or garnet lherzolite as determined by the work of *Walter* [1998]. Rather they appear to have experienced olivine addition since last in equilibrium with a spinel lherzolite or experienced high extents of melting such that they are no longer in equilibrium with a lherzolite assemblage. However, for the sake of comparison, we choose to use the *Putirka et al.* [2007] calculated compositions to contrast thermometric and barometric estimates, rather than attempt to correct a fictive liquid composition for olivine addition.

[36] Pressures for the calculated parental OIB liquids determined with our olivine spinel lherzolite barometer and that of *Lee et al.* [2009] are quite different (Figure 8f). Both

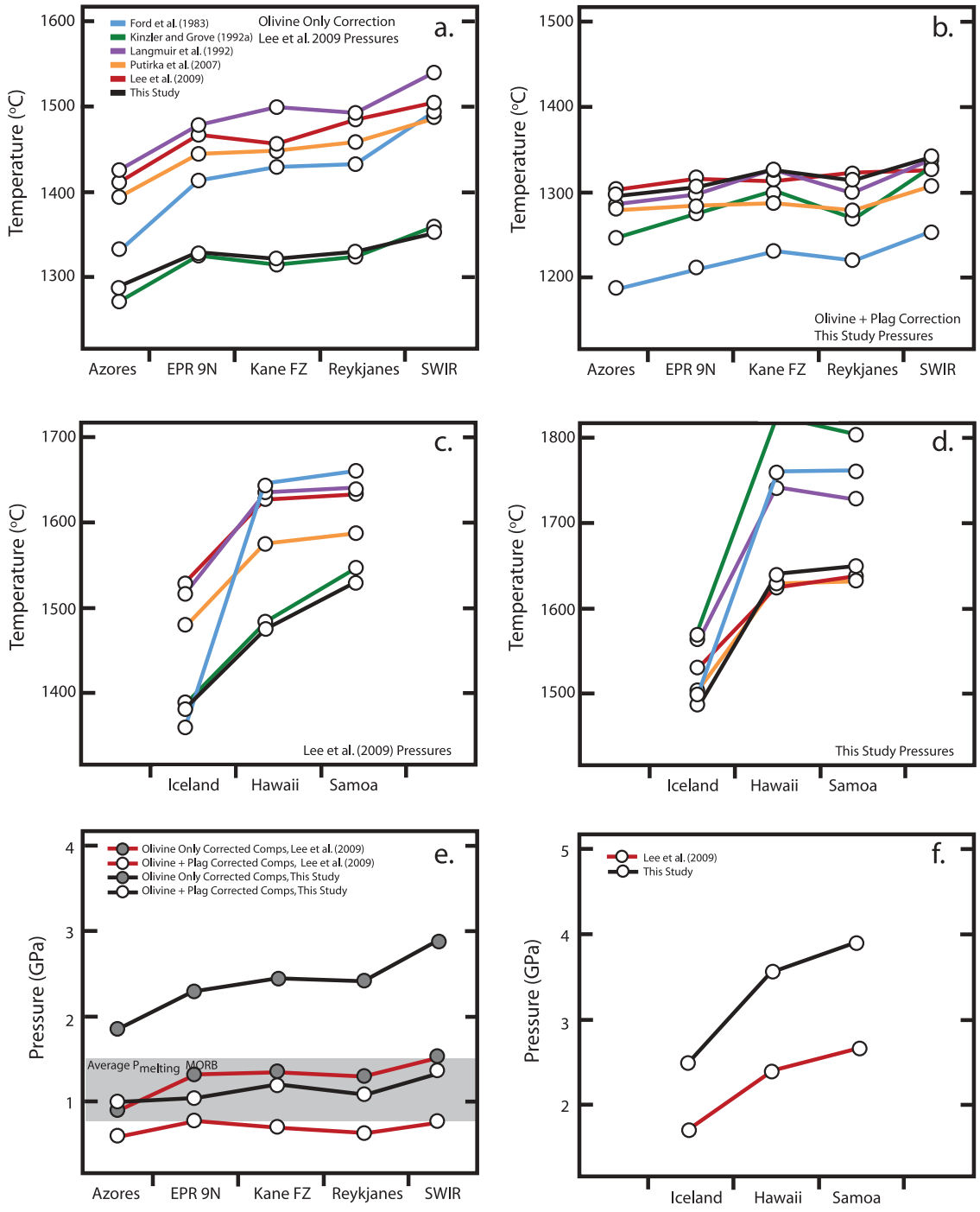

Figure 8. Comparison of temperature estimates from extant thermometers and this study for five MORB and three OIB locations. MORB compositions are primitive glasses from the PetDB database and OIB compositions are calculated by *Putirka et al.* [2007]. Temperatures were calculated using pressure estimates from the *Lee et al.* [2009] barometer and our spinel lherzolite barometer (Table 5).

sets of pressure estimates yield temperature estimates that vary by ~150°C at a given locality (Figures 8c and 8d). All the thermometers yield similar temperature estimates for the Hawaiian and Samoan compositions and temperatures that are ~100–200°C lower for the Icelandic composition depending on the pressure. The thermometer of *Lee et al.* [2009] is not pressure-dependent; therefore the OIB source temperature estimates are identical at either pressure. The parameterization of *Putirka et al.* [2007] is the least pressure sensitive after *Lee et al.* [2009], and an increase in source pressure of ~2 GPa for the Hawaii and Iceland compositions results in an increase of temperatures of ~50°C. At the other end of the spectrum, the parameterization of *Kinzler and Grove* [1992a] is the most pressure-sensitive and an increase in source

Table 7. Geochemistry of Primitive Basalts From Diamond Crater area, Oregon[a]

	DC 07-12	DC 07-13	DC 07-14	DC 07-15	DC 07-16	ch8329	ch8343	ch8357b
Latitude	43.05	43.05	43.05	43.05	43.05	44.9	44.10	43.15
Longitude	−118.43	−118.43	−118.43	−118.43	−118.46	−117.7	−118.60	−118.08
XRF Normalized Major Elements (wt.%):								
SiO_2	47.98	47.90	48.33	48.94	47.83	49.7	47.70	48.00
TiO_2	1.30	1.17	1.25	1.71	1.38	1.25	1.23	0.95
Al_2O_3	17.48	17.71	17.07	15.40	17.18	15.5	15.50	16.50
FeO*	10.11	9.93	10.19	11.89	10.22	9.27	9.81	9.63
MnO	0.18	0.18	0.18	0.22	0.18	0.15	0.17	0.17
MgO	8.71	8.82	8.20	6.74	9.12	9.65	10.30	9.36
CaO	10.72	11.15	11.46	11.38	10.39	9.53	11.10	10.80
Na_2O	2.92	2.71	2.86	3.14	3.01	2.38	2.17	2.44
K_2O	0.40	0.28	0.30	0.39	0.45	0.61	0.78	0.32
P_2O_5	0.22	0.14	0.16	0.20	0.24	0.33	0.31	0.17
Total	99.99	99.20	100.32	99.92	100.22	99.40	100.16	99.41
Mg#	0.61	0.61	0.59	0.50	0.61	0.65	0.65	0.63
ICP-MS Trace Elements (ppm):								
La	7.4	5.0	5.7	7.2	8.3	12.3	16.6	5.3
Ce	17.8	12.3	14.1	18.0	19.9	26.4	33.6	12.7
Pr	2.6	1.9	2.2	2.8	2.9	3.63	4.2	1.9
Nd	12.2	9.3	10.6	13.6	13.5	15.7	17.7	9.0
Sm	3.4	2.8	3.1	4.1	3.7	3.7	4.1	2.6
Eu	1.4	1.1	1.2	1.6	1.4	1.3	1.4	1.0
Gd	3.9	3.3	3.7	5.0	4.1	3.9	4.2	3.1
Tb	0.7	0.6	0.7	0.9	0.7	0.6	0.7	0.6
Dy	4.4	3.9	4.3	5.7	4.5	3.9	4.3	3.8
Ho	0.9	0.8	0.9	1.2	0.9	0.8	0.9	0.8
Er	2.6	2.3	2.5	3.4	2.6	2.2	2.3	2.2
Tm	0.4	0.3	0.4	0.5	0.4	0.3	0.3	0.3
Yb	2.3	2.1	2.3	3.1	2.4	1.9	2.2	2.1
Lu	0.4	0.3	0.4	0.5	0.4	0.3	0.3	0.3
Ba	193.5	144.2	154.8	199.5	203.5	254.7	268.6	157.7
Th	0.5	0.3	0.4	0.4	0.5	1.0	2.3	0.6
Nb	5.8	3.4	4.2	5.1	6.9	12.1	26.5	4.1
Y	22.9	20.6	22.7	30.5	23.5	20.8	22.2	20.2
Hf	2.3	1.8	2.0	2.6	2.5	2.0	2.5	1.7
Ta	0.4	0.2	0.3	0.3	0.4			
U	0.2	0.1	0.1	0.2	0.2	0.3	0.6	0.1
Pb	0.9	0.9	0.8	1.0	1.0	2.6	1.5	0.9
Rb	4.2	3.0	3.2	3.7	5.0	7.1	17.3	2.5
Cs	0.1	0.0	0.0	0.1	0.1	0.2	0.1	0.02
Sr	308.9	272.7	274.0	253.6	321.1	397.6	314.6	223.2
Sc	31.2	34.2	41.0	47.9	30.2	29.4	33.9	34.8
Zr	90.4	66.6	74.1	99.1	101.5	76.4	97.5	65.5
Ba/Nb	33.3	42.3	36.5	38.9	29.6	21.0	10.1	38.1

[a]Major element XRF and trace element ICPMS analyses were conducted at the WSU GeoAnalytical Lab.

pressure of ~2 GPa results in an increase of temperatures of ~300°C. The pressure-dependence of the remaining thermometers falls between these two end-members, with our model tending toward more pressure-dependent. It is difficult to draw conclusions about the actual source temperature and pressure for the three OIB localities from these calculations, which reinforces the observation that the determination of the parental liquid compositions and estimates of source pressure have profound effects on the temperature estimates for OIB genesis.

9. Case Study of Basaltic Lavas From Oregon's High Lava Plains (HLP)

[37] A suite of primitive basaltic lavas from Diamond Crater and surroundings in Oregon's eastern HLP were selected to demonstrate the utility of our model. Trace element modeling of the basalt geochemistry is first employed to determine whether these basalts originated from a primitive mantle source. We then apply our thermometer and barometer to the fractionation-corrected Diamond Crater parental liquid compositions to determine the conditions they were last in equilibrium with an upper mantle phase assemblage. Finally, the Diamond Crater parental liquids are compared to the composition of predicted batch and near-fractional melts of both fertile and depleted lherzolite mantle bulk compositions produced at the pressures and temperatures calculated for the Diamond Crater liquids.

[38] Diamond Crater (43°05′N, 118°43′W) is a suite of basaltic lava flows [*Russell and Nicholls*, 1987] emplaced around a central vent between 8,400 and 6,400 yrs. ago (Sherrod, written communication, 2009). The lavas are diktytaxitic high alumina olivine tholeiites (HAOT) containing <2 volume % of olivine and plagioclase phenocrysts (visible in hand sample) and Mg#'s of 0.50–0.65. Major and trace element geochemistry of all samples presented here were conducted at the Washington State University GeoAnalytical Lab (Table 7). In addition, electron microprobe analyses of the phenocrysts and chilled-glass groundmass of samples from Diamond Crater were conducted at the

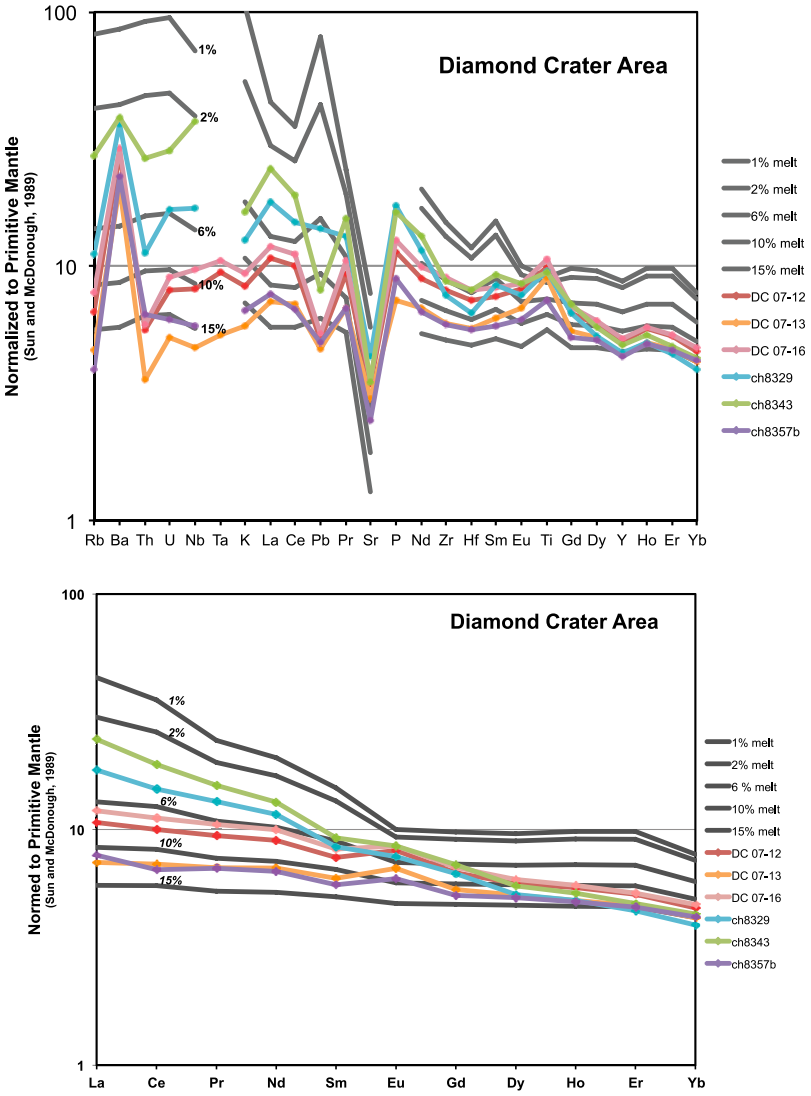

Figure 9. (top) Trace element abundance of basalts from the Diamond Crater region, Oregon and modeled 1–15% melts of a spinel lherzolite mantle. (bottom) Rare earth element abundances of the same samples and modeled melts.

Massachusetts Institute of Technology following the same analytical procedures outlined for the experiments presented in section 3.

[39] The trace element abundances in the most primitive Diamond Crater samples are compared to modeled 1–15% batch melts of a primitive spinel lherzolite mantle in Figure 9. We modeled batch melting of primitive upper mantle using the appropriate equations from *Shaw* [2006], major element abundances from *Hart and Zindler* [1986], trace element abundances from *Hoffmann* [1988], partition coefficients from *Halliday et al.* [1995] with additional spinel partition coefficients from *Canil* [2004] and *Kinzler and Grove* [1992a] and mantle modes and melting reactions from *Kinzler* [1997]. The light rare earth element abundances (REE) produced by this model suggests samples ch8329 and ch8343 are similar to 2–6 wt.% melts of a primitive spinel lherzolite mantle, samples DC 07–16 and DC 07–12 are closely matched by 6–10 wt.% melts and DC 07–13 and ch8357b are consistent with 10–15 wt.% melts. On the other hand, the heavier REE abundances suggest 10–15 wt.% melting for all the samples. All samples are relatively enriched in Ba, Sr and La, which are typically carried by subduction zone fluids or melts and depleted in Rb, Th and Pb relative to fertile mantle melts of varying extent. Together, these trace element abundances may be the result of low percentage melting of a depleted mantle that has been metasomatically enriched in LREE and large ion lithophile elements (LILE). The positive or negligible Eu-anomaly demonstrates these samples were not a product of melting plagioclase lherzolite. Compositional variability in these aphyric lavas, as well as the chemical composition of the plagioclase and olivine phenocrysts in the Diamond Crater samples indicate these liquids experienced crystallization at near anhydrous conditions. Thus these samples are excellent candidates for our model because they appear to be nominally anhydrous low extent melts of spinel lherzolite mantle that may have experienced some degree of depletion followed by metasomatic enrichment of LREE and LILE.

Table 8. Starting Compositions, Run Conditions and Results From the Spinel Lherzolite Forward Melting Model, as Used to Replicate the Parental Liquids for Basaltic Lavas From the Diamond Crater area, Oregon[a]

	Melting Style	Total F	dF/dP	SiO_2	TiO_2	Al_2O_3	Cr_2O_3	FeO	MgO	CaO	Na_2O	K_2O	T (°C)	P (GPa)
Patagonia xenolith				45.00	0.06	1.65		8.80	43.60	1.32	0.14	0.02		
H & Z primitive mantle				46.16	0.18	4.08	0.47	7.58	37.94	3.22	0.33	0.032		
Patagonia Xenolith														
1.8-1.3 GPa	Near-Fractional	6%	1%/0.1 GPa	47.27	0.41	16.57	0.13	8.94	12.83	11.83	1.64	0.38		
1.6-1.0 GPa	Near-Fractional	6%	1%/0.1 GPa	47.97	0.34	16.98	0.13	8.42	12.11	12.01	1.72	0.33		
1.3 GPa	Batch	6%		47.82	0.31	16.96	0.14	8.28	12.40	12.28	1.49	0.32	1329	1.3
1.3 GPa	Batch	8%		47.68	0.29	16.80	0.15	8.25	12.76	12.54	1.29	0.24	1332	1.3
1.6 GPa	Batch	4%		47.14	0.40	16.65	0.13	8.85	12.94	11.84	1.58	0.47	1363	1.6
1.6 GPa	Batch	6%		46.92	0.36	16.40	0.14	8.93	13.41	12.15	1.36	0.32	1366	1.6
H & Z Primitive Mantle														
1.8-1.3 GPa	Near-Fractional	6%	1%/0.1 GPa	48.98	1.03	17.43	0.09	7.87	10.72	9.94	3.31	0.61		
1.6-1.0 GPa	Near-Fractional	6%	1%/0.1 GPa	49.73	0.87	18.00	0.10	7.29	9.94	9.98	3.57	0.52		
1.3 GPa	Batch	6%		49.23	0.81	17.76	0.10	7.44	10.56	10.64	2.97	0.50	1319	1.3
1.3 GPa	Batch	8%		48.89	0.77	17.54	0.11	7.57	11.04	11.07	2.64	0.38	1323	1.3
1.6 GPa	Batch	6%		48.25	0.95	17.15	0.10	8.13	11.58	10.62	2.72	0.50	1357	1.6
Fractionation-Corrected Diamond Crater Area Samples														
DC 07-12				46.90	0.78	19.56		7.64	11.53	10.94	2.29	0.24	1359	1.57
DC 07-13				46.84	0.73	19.64		7.68	11.44	11.26	2.15	0.17	1349	1.48
DC 07-14				46.94	0.72	19.55		7.59	11.37	11.45	2.17	0.17	1342	1.42
DC 07-15				46.70	0.75	19.55		7.75	11.54	11.38	2.08	0.17	1349	1.47
DC 07-16				46.92	0.84	19.28		7.76	11.72	10.68	2.39	0.27	1370	1.67
ch8329				48.95	0.87	18.38		7.50	11.12	10.43	2.08	0.43	1351	1.51
ch8343				47.11	0.84	18.54		7.73	11.58	11.62	1.83	0.53	1344	1.44
ch8357b				47.49	0.61	19.53		7.44	11.14	11.45	2.02	0.21	1333	1.34

[a]Starting bulk peridotite compositions used in the modeling are a xenolith of depleted metasomatized mantle from Patagonia [*Ntaflos et al.*, 2007] and the primitive mantle composition of *Hart and Zindler* [1986], renormalized to exclude MnO, NiO and P_2O_5. The Diamond Crater compositions were corrected for olivine + plagioclase fractionation using the methods discussed in Section VI until they reached equilibrium with Fo90 olivine. Pressure and temperature estimates for Diamond Crater area samples were calculated with the spinel lherzolite thermometer and barometer in Table 5.

[40] For use in our model, the major element compositions of the selected samples were first corrected for minor fractional crystallization following the methods discussed in section 7.1. The presence of either olivine + plagioclase phenocrysts or microphenocrysts in the Diamond Crater samples and the chemical composition of these minerals imply these samples experienced a period of low pressure olivine + plagioclase fractionation. Alternatively, we tested correcting the samples for a period of olivine-only fractionation, followed by a period of lower pressure olivine + plagioclase fractionation. However, correcting for this scenario drives the liquids toward the olivine apex on a Plag-Cpx-Oliv ternary and beyond the spinel MSP long before they reach equilibrium with Fo90 olivine. Therefore we conclude, the most logical fractional crystallization history for these samples is a period of low-pressure olivine + plagioclase fractionation, and only a minor amount of olivine addition is needed to bring them into saturation with a spinel lherzolite assemblage.

[41] Once corrected for fractional crystallization, the compositions and their corresponding mineral component values were used as inputs for our spinel lherzolite barometer and thermometer (Table 5) and the results are presented in Table 8. The samples were generated at temperatures of ~1333–1370°C and pressures of 1.34–1.67 GPa, which corresponds to depths of ~45–56 km based on preliminary density models for the crust and mantle from recent seismic refraction profiles near Diamond Crater (Cox, personal communication, 2011). Recent work on the crustal structure of Oregon's HLP using teleseismic P-to-S receiver functions finds the Moho is located at ~30 km in the region of Diamond Crater when the H-κ method is applied to individual stations, or ~36 km if the maximum amplitudes from GCCP stacks are used [*Eagar et al.*, 2011]. In either case, the primitive basalts erupted in the Diamond Crater area appear to be formed by shallow decompression melting of metasomatized spinel lherzolite, with the shallowest depths of melting ~10–15 km below the Moho.

[42] We can also apply our forward model of spinel lherzolite melting to model both batch and near-fractional mantle melting over the range of calculated depths for the Diamond Crater parental liquids. We specified the bulk mantle composition in our models to be either that of the primitive mantle from *Hart and Zindler* [1986] or a xenolith of depleted lithospheric mantle with re-enriched LREE from southern Patagonia [*Ntaflos et al.*, 2007]. Models were run with initial pressures of 1.0 to 1.8 GPa, an olivine-melt $K_D^{Fe\text{-}Mg}$ of 0.3, and either 100% of the melt was removed for batch melting or 90% in the case of near-fractional melting. Batch melting models were run for 2–10 wt.% melting. For near-fractional melting, we chose the melt production rate (dF/dP) to be 1% per 0.1 GPa of decompression and track the composition of the melt produced at each step, as well as the accumulated melt. The modeling results that best replicate the composition of the fractionation-corrected Diamond Crater basaltic lavas are presented in Figure 10 and Table 8. The Diamond Crater liquids are bracketed by the model melts of the Patagonia xenolith and the primitive mantle bulk compositions in oxide-oxide composition space (Figure 10). The Patagonia xenolith bulk composition yields melts that are lower in SiO_2 and Na_2O and higher in CaO, FeO and MgO relative to the Diamond Crater liquids, whereas the primitive

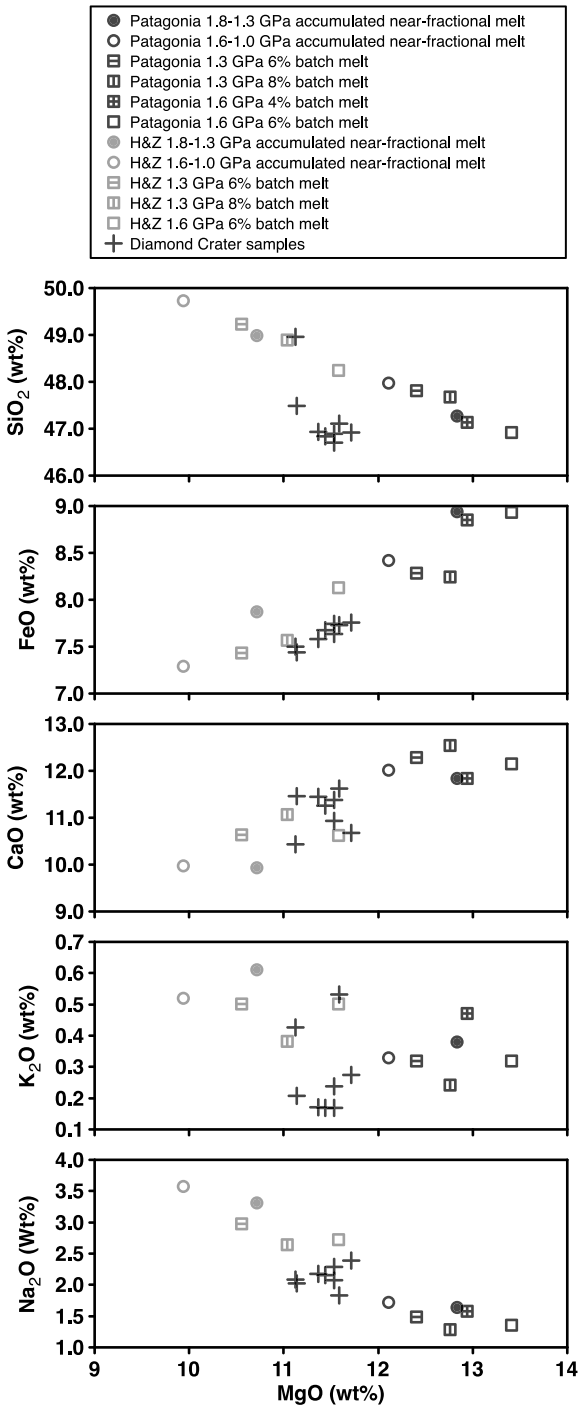

Figure 10. Results of our forward spinel lherzolite melting model relative to fractionation-corrected basaltic liquids from the Diamond Crater area, Oregon.

mantle bulk composition produces the opposite result. Overall the major element modeling suggests the source of the Diamond Crater liquids was less depleted than the Patagonia lithospheric xenolith but more depleted than primitive mantle, as evidenced by their MgO contents. Although the Diamond Crater liquids tend to be lower in K_2O than melts produced from either of the model mantle compositions, the trace element concentrations indicate the mantle source was enriched in the LILE elements and LREE and argue for metasomatic enrichment following an overall depletion event. While there is not a definitive result as to whether the Diamond Crater liquids originated via batch or fractional melting processes, 1.6 GPa 6% or 1.3 GPa 8% batch melts of a mantle source with a major element composition between that of the primitive mantle and depleted xenolith would yield the best fit to the Diamond Crater liquids and fall within $\ll$1 wt.% of the key oxides (Figure 10). An increasing number of studies on HAOT magma generation at continent margins and interiors [e.g., *Bartels et al.*, 1991; *Bacon et al.*, 1997; *Holbig and Grove*, 2008] suggest that HAOTs likely form under batch melting conditions near the Moho, similar to our results.

[43] Overall these two completely independent sets of calculations (i.e., the thermo-barometric calculations and the forward mantle melting model) both suggest the Diamond Crater basalts were generated during small degrees of melting at ~1.3–1.6 GPa of a spinel lherzolite that has been depleted in most major elements relative to primitive mantle and the trace element modeling suggests a post-depletion enrichment in LILE and LREE as expected during subduction-related metasomatism. This example also illustrates how our spinel lherzolite forward melting model can be used to constrain the melting style, in addition to the pressure, temperature and composition of the bulk mantle during melting. Thus the plagioclase and spinel lherzolite melting models presented here represent two new tools to understand the melting of mantle with non-MORB source bulk compositions and the petrogenesis of HAOT magmas.

10. Conclusions

[44] Following the application of our thermometer and barometer to MORB, OIB, and intraplate basalts the question arises: what situations are our thermometer and barometer best suited to? As demonstrated in section 7.1, it is of critical importance to have a quantitative model to correct any nominally anhydrous primitive basaltic liquid for the effects of fractional crystallization prior to thermobarometric calculations. In addition, it appears our thermometer and barometer are well suited to calculating the temperature of both MORB and intraplate basalts, like those from Diamond Crater, Oregon because of the range of melt compositions used to calibrate the model. Because the model is calibrated with only experiments that contain all of the nominally anhydrous mantle phases, our model is appropriate for use with low to intermediate degree melts (<20 wt.%, which is approximately the location of cpx-out) of the lherzolite mantle, and not those that may have originated from a harzburgitic or pyroxenitic mantle, such as the Hawaiian basalts [*Wagner and Grove*, 1998; *Stolper et al.*, 2004], or parental OIB liquids that have either experienced crystal accumulation or higher extents of melting. In particular, the model is well suited to examining the genesis of intraplate HAOT's such as those from Diamond Crater, Oregon where the mantle has a bulk composition that has been modified by subduction and melt extraction.

[45] **Acknowledgments.** This work benefited from discussions with Jay Barr and Mark Behn and the thoughtful reviews of Keith Putirka, Didier LaPorte, and an anonymous reviewer. Support for this work was provided by National Science Foundation grants EAR-0507486, EAR-0538179, and

EAR-1118598. We would also like to thank Thresa Geisler and Robert Renchler at the Bureau of Land Management for permission to collect samples in the Diamond Crater Outstanding Natural Area, Oregon.

References

Armstrong, J. T. (1995), CITZAF–A package of correction programs for the quantitative electron microbeam X-ray analysis of thick polished materials, thin-films, and particles, *Microbeam Anal.*, *4*, 177–200.

Asimow, P. D., and J. Longhi (2004), The significance of multiple saturation points in the context of polybaric near-fractional melting, *J. Petrol.*, *45*, 2349–2367, doi:10.1093/petrology/egh043.

Asimow, P. D., M. M. Hirschmann, and E. M. Stolper (1997), An analysis of variations in isentropic melt productivity, *Philos. Trans. R. Soc. A*, *355*, 255–281, doi:10.1098/rsta.1997.0009.

Bacon, C. R., P. E. Bruggman, R. L. Christiansen, M. A. Clynne, J. D. Donnelly Nolan, and W. Hildreth (1997), Primitive magmas at five Cascade volcanic fields: Melts from hot, heterogeneous sub-Arc mantle, *Can. Mineral.*, *35*, 397–423.

Baker, M. B., and E. M. Stolper (1994), Determining the composition of high-pressure mantle melts using diamond aggregates, *Geochim. Cosmochim. Acta*, *58*(13), 2811–2827, doi:10.1016/0016-7037(94)90116-3.

Baker, M. B., T. L. Grove, and R. Price (1994), Primitive basalts and andesites from the Mt. Shasta region, N California: Products of varying melt fraction and water-content, *Contrib. Mineral. Petrol.*, *118*, 111–129, doi:10.1007/BF01052863.

Baker, M. B., M. M. Hirschmann, M. S. Ghiorso, and E. M. Stolper (1995), Composition of near-solidus peridotite melts from experiments and thermodynamic calculations, *Nature*, *375*, 308–311, doi:10.1038/375308a0.

Bartels, K. S., R. J. Kinzler, and T. L. Grove (1991), High pressure phase relations of primitive high-alumina basalts from Medicine Lake volcano, northern California, *Contrib. Mineral. Petrol.*, *108*, 253–270, doi:10.1007/BF00285935.

Boyd, F. R., and J. L. England (1960), Apparatus for phase equilibrium studies at pressures up to 50 kilobars and temperatures up to 1750°C, *J. Geophys. Res.*, *65*, 741–748, doi:10.1029/JZ065i002p00741.

Canil, D. (2004), Midly incompatible elements in peridotites and the origins of mantle lithosphere, *Lithos*, *77*, 375–393, doi:10.1016/j.lithos.2004.04.014.

Desonie, D. L., R. A. Duncan, and J. H. Natland (1993), Temporal and geochemical variability of volcanic products of the Marquesas hotspot, *J. Geophys. Res.*, *98*, 17,649–17,665, doi:10.1029/93JB01562.

Dick, H. J. B., R. L. Fischer, and W. B. Bryan (1984), Mineralogic variability of the uppermost mantle along mid-ocean ridges, *Earth Planet. Sci. Lett.*, *69*, 88–106, doi:10.1016/0012-821X(84)90076-1.

Draper, D. S., and A. D. Johnston (1992), Anhydrous PT phase relations of an Aleutian high-MgO basalt: An investigation of the role of olivine-liquid reaction in the generation of arc high-alumina basalts, *Contrib. Mineral. Petrol.*, *112*, 501–519, doi:10.1007/BF00310781.

Dunn, T., and C. Sen (1994), Mineral/matrix partition-coefficients for ortho-pyroxene, plagioclase, and olivine in basaltic to andesitic systems: A combined analytical and experimental study, *Geochim. Cosmochim. Acta*, *58*, 717–733, doi:10.1016/0016-7037(94)90501-0.

Eagar, K. C., M. J. Fouch, D. E. James, and R. W. Carlson (2011), Crustal structure beneath the High Lava Plains of eastern Oregon and surrounding regions from receiver function analysis, *J. Geophys. Res.*, *116*, B02313, doi:10.1029/2010JB007795.

Elkins-Tanton, L. T., T. L. Grove, and J. Donnelly-Nolan (2001), Hot, shallow melting under the Cascades volcanic arc, *Geology*, *29*, 631–634, doi:10.1130/0091-7613(2001)029<0631:HSMMUT>2.0.CO;2.

Falloon, T. J., D. H. Green, H. S. C. O'Neill, and W. O. Hibberson (1997), Experimental tests of low degree peridotite partial melt compositions: Implications for the nature of anhydrous near-solidus peridotite melts at 1 GPa, *Earth Planet. Sci. Lett.*, *152*, 149–162, doi:10.1016/S0012-821X(97)00155-6.

Falloon, T. J., L. V. Danyushevsky, and D. H. Green (2001), Peridotite melting at 1 GPa: Reversal experiments on partial melt compositions produced by peridotite-basalt sandwich experiments, *J. Petrol.*, *42*, 2363–2390, doi:10.1093/petrology/42.12.2363.

Falloon, T. J., D. H. Green, L. V. Danyushevsky, and A. W. McNeill (2008), The composition of near-solidus partial melts of fertile peridotite at 1 and 1.5 GPa: Implications for the petrogenesis of MORB, *J. Petrol.*, *49*, 591–613, doi:10.1093/petrology/egn009.

Ford, C. E., D. G. Russel, J. A. Craven, and M. R. Fisk (1983), Olivine-liquid equilibria: Temperature, pressure and composition dependence of the crystal/liquid cation partition coefficients for Mg, Fe2+, Ca and Mn, *J. Petrol.*, *24*, 256–265.

Gaetani, G. A., and T. L. Grove (1998), The influence of water on melting of mantle peridotite, *Contrib. Mineral. Petrol.*, *131*, 323–346, doi:10.1007/s004100050396.

Green, D. H. (1973), Experimental melting studies on a model upper mantle composition at high-pressure under water-saturated and water-undersaturated conditions, *Earth Planet. Sci. Lett.*, *19*, 37–53, doi:10.1016/0012-821X(73)90176-3.

Gregg, P. M., M. D. Behn, J. Lin, and T. L. Grove (2009), Melt generation, crystallization, and extraction beneath segmented oceanic transform faults, *J. Geophys. Res.*, *114*, B11102, doi:10.1029/2008JB006100.

Grove, T. L. (1993), Corrections to expression for calculating mineral components in "Origin of calc-alkaline series lavas at Medicine Lake Volcano by fractionation, assimilation and mixing" and "Experimental petrology of normal MORB near the Kane Fracture Zone: 22°–25°N, mid-Atlantic ridge", *Contrib. Mineral. Petrol.*, *114*, 422–424, doi:10.1007/BF01046543.

Grove, T. L., and T. C. Juster (1989), Experimental investigations of low-Ca pyroxene stability and olivine-pyroxene-liquid equilibria at 1-atm in natural basaltic and andesitic liquids, *Contrib. Mineral. Petrol.*, *103*, 287–305, doi:10.1007/BF00402916.

Grove, T. L., R. J. Kinzler, and W. B. Bryan (1992), Fractionation of Mid-Ocean Ridge Basalt (MORB), in *Mantle Flow and Melt Generation at Mid-Ocean Ridges*, *Geophys. Monogr. Ser.*, vol. 71, edited by J. P. Morgan, D. K. Blackman, and J. M. Sinton, pp. 281–310, AGU, Washington, D. C., doi:10.1029/GM071p0281.

Grove, T. L., N. Chatterjee, S. W. Parman, and E. Médard (2006), The influence of H_2O on mantle wedge melting, *Earth Planet. Sci. Lett.*, *249*, 74–89, doi:10.1016/j.epsl.2006.06.043.

Halliday, A. N., D.-C. Lee, S. Tommasini, G. R. Davies, C. R. Paslick, J. G. Fitton, and D. E. James (1995), Incompatible trace elements in OIB and MORB and source enrichment in the sub-oceanic mantle, *Earth Planet. Sci. Lett.*, *133*, 379–395, doi:10.1016/0012-821X(95)00097-V.

Hart, S. R., and A. Zindler (1986), In search of a bulk-Earth composition, *Chem. Geol.*, *57*, 247–267, doi:10.1016/0009-2541(86)90053-7.

Hauri, E. (2002), SIMS analysis of volatiles in silicate glasses, 2: Isotopes and abundances in Hawaiian melt inclusions, *Chem. Geol.*, *183*, 115–141, doi:10.1016/S0009-2541(01)00374-6.

Hauri, E., G. A. Gaetani, and T. Green (2006), Partitioning of water during melting of the Earth's upper mantle at H_2O-undersaturated conditions, *Earth Planet. Sci. Lett.*, *248*, 715–734, doi:10.1016/j.epsl.2006.06.014.

Hays, J. F. (1966), Lime-alumina-silica, *Carnegie Inst. of Wash. Yearb.*, *65*, 234–239.

Herzberg, C., and P. D. Asimow (2008), Petrology of some oceanic island basalts: PRIMELT2.XLS software for primary magma calculation, *Geochem. Geophys. Geosyst.*, *9*, Q09001, doi:10.1029/2008GC002057.

Herzberg, C., P. D. Asimow, N. Arndt, Y. Niu, C. E. Lesher, J. G. Fitton, M. J. Cheadle, and A. D. Saunders (2007), Temperatures in ambient mantle and plumes: Constraints from basalts, picrites and komatiites, *Geochem. Geophys. Geosyst.*, *8*, Q02006, doi:10.1029/2006GC001390.

Hirose, K., and T. Kawamoto (1995), Hydrous partial melting of lherzolite at 1 GPa: The effect of H_2O on the genesis of basaltic magmas, *Earth Planet. Sci. Lett.*, *133*, 463–473, doi:10.1016/0012-821X(95)00096-U.

Hirschmann, M. M., M. S. Ghiorso, F. A. Davis, S. M. Gordon, D. Mukherjee, T. L. Grove, M. Krawczynski, E. Médard, and C. B. Till (2008), Library of Experimental Phase Relations (LEPR): A database and web portal for experimental magmatic phase equilibria data, *Geochem. Geophys. Geosyst.*, *9*, Q03011, doi:10.1029/2007GC001894.

Hoffmann, A. W. (1988), Chemical differentiation of the Earth: The relationship between mantle, continental crust, and oceanic crust, *Earth Planet. Sci. Lett.*, *90*, 297–314, doi:10.1016/0012-821X(88)90132-X.

Holbig, E. S., and T. L. Grove (2008), Mantle melting beneath the Tibetan Plateau: Experimental constraints on the generation of ultra-potassic lavas from Qiangtang, Tibet, *J. Geophys. Res.*, *113*, B04210, doi:10.1029/2007JB005149.

Johnson, K. T. M., H. J. B. Dick, and N. Shimizu (1990), Melting in the oceanic mantle: An ion microprobe study of diopsides in abyssal peridotites, *J. Geophys. Res.*, *95*, 2661–2678, doi:10.1029/JB095iB03p02661.

Kinzler, R. J. (1997), Melting of mantle peridotite at pressures approaching the spinel to garnet transition: Application to mid-ocean ridge basalt petrogenesis, *J. Geophys. Res.*, *102*, 853–874, doi:10.1029/96JB00988.

Kinzler, R. J., and T. L. Grove (1992a), Primary magmas of Midocean Ridge basalts: 1. Experiments and methods, *J. Geophys. Res.*, *97*, 6885–6906, doi:10.1029/91JB02840.

Kinzler, R. J., and T. L. Grove (1992b), Primary Magmas of Midocean Ridge Basalts: 2. Applications, *J. Geophys. Res.*, *97*, 6907–6926, doi:10.1029/91JB02841.

Kinzler, R. J., and T. L. Grove (1993), Corrections and further discussion of the primary magmas of Mid-Ocean Ridge basalts, 1 and 2, *J. Geophys. Res.*, *98*, 22,339–22,347, doi:10.1029/93JB02164.

Kinzler, R. J., and T. L. Grove (1999), Origin of depleted cratonic harzburgite by deep fractional melt extraction and shallow olivine cumulate

infusion, in Proceedings of the 7th International Kimberlite Conference, edited by J. J. Gurney, pp. 437–443, Red Roof Design, Cape Town.

Klein, E. M., and C. H. Langmuir (1987), Global correlations of ocean ridge basalt chemistry and axial depth and crustal thickness, *J. Geophys. Res.*, *92*, 8089–8115, doi:10.1029/JB092iB08p08089.

Klein, E. M., and C. H. Langmuir (1989), Local versus global variations in ocean ridge composition: A reply, *J. Geophys. Res.*, *94*, 4241–4252, doi:10.1029/JB094iB04p04241.

Kushiro, I. (1975), On the nature of silicate melt and its significance in magma genesis: Regularities in the shift of the liquidus boundaries involving olivine, pyroxene, and silica minerals, *Am. J. Sci.*, *275*, 411–431, doi:10.2475/ajs.275.4.411.

Kushiro, I. (1990), Partial melting of the mantle wedge and evolution of island arc crust, *J. Geophys. Res.*, *95*, 15,929–15,939, doi:10.1029/JB095iB10p15929.

Kushiro, I. (1996), Partial melting of a fertile mantle peridotite at high pressures: An updated experimental study using aggregates of diamond, in *Earth Processes: Reading the Isotopic Code*, *Geophys. Monogr. Ser.*, vol. 95, edited by A. Basu and S. Hart, pp. 109–122, AGU, Washington, D. C., doi:10.1029/GM095p0109

Kushiro, I., and H. S. J. Yoder (1966), Anorthite-forsterite and anorthite-enstatite reactions and their bearing on the basalt-eclogite transformation, *J. Petrol.*, *7*, 337–362.

Kushiro, I., Y. Synono, and S. Akimoto (1968), Melting of a peridotite nodule at high pressures and high water pressures, *J. Geophys. Res.*, *73*, 6023–6029, doi:10.1029/JB073i018p06023.

Langmuir, C. H., E. M. Klein, and T. Plank (1992), Petrological systematics of Mid-Ocean Ridge basalts: Constraints on melt generation beneath ocean ridges, in *Mantle Flow and Melt Generation at Mid-Ocean Ridges*, *Geophys. Monogr. Ser.*, vol. 71, edited by J. Phipps Morgan, D. K. Blackman, and J. M. Sinton, pp. 183–280, AGU, Washington, D. C., doi:10.1029/GM071p0183.

Laporte, D., M. J. Toplis, M. Seyler, and J.-L. Devidal (2004), A new experimental technique for extracting liquids from peridotite at very low degrees of melting: Application to partial melting of depleted peridotite, *Contrib. Mineral. Petrol.*, *146*, 463–484, doi:10.1007/s00410-003-0509-3.

Lee, C. T. A., P. Luffi, T. Plank, H. Dalton, and W. P. Leeman (2009), Constraints on the depths and temperatures of basaltic magma generation on Earth and other terrestrial planets using new thermobarometers for mafic magmas, *Earth Planet. Sci. Lett.*, *279*, 20–33, doi:10.1016/j.epsl.2008.12.020.

Longhi, J. (1991), Comparative liquidus equilibria of hypersthene-normative basalts at low pressure, *Am. Mineral.*, *76*, 785–800.

Longhi, J. (2005), Temporal stability and pressure calibration of barium carbonate and talc/pyrex pressure media in a piston-cylinder apparatus, *Am. Mineral.*, *90*, 206–218, doi:10.2138/am.2005.1348.

McKenzie, D., and M. J. Bickle (1988), The volume and composition of melt generated by extension of the lithosphere, *J. Petrol.*, *29*, 625–679.

Médard, E., C. A. McCammon, J. A. Barr, and T. L. Grove (2008), Oxygen fugacity, temperature reproducibility, and H_2O contents of nominally anhydrous piston-cylinder experiments using graphite capsules, *Am. Mineral.*, *93*, 1838–1844, doi:10.2138/am.2008.2842.

Meen, J. K. (1990), Elevation of potassium content of basaltic magma by fractional crystallization: The effect of pressure, *Contrib. Mineral. Petrol.*, *104*, 309–331, doi:10.1007/BF00321487.

Niu, Y., and R. Batiza (1991), An empirical method for calculating melt compositions produced beneath Mid-Ocean Ridges: Applications for axis and off-axis (seamounts), melting, *J. Geophys. Res.*, *96*, 21,753–21,777, doi:10.1029/91JB01933.

Ntaflos, T., E. A. Bjerg, C. H. Labudia, and G. Kurat (2007), Depleted lithosphere from the mantle wedge beneath Tres Lagos, southern Patagonia, Argentina, *Lithos*, *94*, 46–65, doi:10.1016/j.lithos.2006.06.011.

Pichavant, M., B. O. Mysen, and R. MacDonald (2002), Source and H_2O content of high-MgO magmas in island arc settings: An experimental study of a primitive calc-alkaline basalt from St. Vincent, Lesser Antilles arc, *Geochim. Cosmochim. Acta*, *66*, 2193–2209, doi:10.1016/S0016-7037(01)00891-2.

Pickering-Witter, J., and A. D. Johnston (2000), The effects of variable bulk composition on the melting systematics of fertile peridotitic assemblages, *Contrib. Mineral. Petrol.*, *140*, 190–211, doi:10.1007/s004100000183.

Presnall, D. C., J. R. Dixon, T. H. O'Donnell, and S. A. Dixon (1979), Generation of Mid-Ocean Ridge tholeiites, *J. Petrol.*, *20*, 3–35.

Putirka, K. D. (2005), Mantle potential temperature at Hawaii, Iceland, and the mid-ocean ridge system, as inferred from olivine phenocrysts: Evidence for thermally driven mantle plumes, *Geochem. Geophys. Geosyst.*, *6*, Q05L08, doi:10.1029/2005GC000915.

Putirka, K. D., M. R. Perfit, F. J. Ryerson, and M. G. Jackson (2007), Ambient and excess mantle temperatures, olivine thermometry, and active vs. passive upwelling, *Chem. Geol.*, *241*, 177–206, doi:10.1016/j.chemgeo.2007.01.014.

Robinson, J. A. C., B. J. Wood, and J. D. Blundy (1998), The beginning of melting of fertile and depleted peridotite at 1.5 GPa, *Earth Planet. Sci. Lett.*, *155*, 97–111, doi:10.1016/S0012-821X(97)00162-3.

Russell, J., and J. Nicholls (1987), Early crystallization history of alkali olivine basalts, Diamond Crater, Oregon, *Geochim. Cosmochim. Acta*, *51*(1), 143–154.

Schwab, B. E., and A. D. Johnston (2001), Melting systematics of modally variable, compositionally intermediate peridotites and the effects of mineral fertility, *J. Petrol.*, *42*, 1789–1811, doi:10.1093/petrology/42.10.1789.

Shaw, D. M. (2006), *Trace Elements in Magmas: A Theoretical Treatment*, 243 pp., Cambridge Univ. Press, Cambridge, U. K.

Sisson, T. W., and T. L. Grove (1993), Temperatures and H_2O contents of low-MgO high-alumina basalts, *Contrib. Mineral. Petrol.*, *113*, 167–184, doi:10.1007/BF00283226.

Spear, F. S. (1993), *Metamorphic Phase Equilibria and Pressure-Temperature-Time Paths*, Mineral. Soc. of Am., Washington, D. C.

Stolper, E. M., S. Sherman, M. Garcia, M. Baker, and C. Seaman (2004), Glass in the submarine section of the HSDP2 drill core, Hilo, Hawaii, *Geochem. Geophys. Geosyst.*, *5*, Q07G15, doi:10.1029/2003GC000553.

Takagi, D., H. Sato, and N. Nakagawa (2005), Experimental study of a low-alkali tholeiite at 1.5 kbar: Optimal condition for the crystallization of high-An plagioclase in hydrous arc tholeiite, *Contrib. Mineral. Petrol.*, *149*, 527–540, doi:10.1007/s00410-005-0666-7.

Till, C. B., T. L. Grove, and A. C. Withers (2012), The beginnings of hydrous mantle wedge melting, *Contrib. Mineral. Petrol.*, *163*, 669–688, doi:10.1007/s00410-011-0692-6.

Toplis, M. J. (2005), The thermodynamics of iron and magnesium partitioning between olivine and liquid: Criteria for assessing and predicting equilibrium in natural and experimental systems, *Contrib. Mineral. Petrol.*, *149*, 22–39, doi:10.1007/s00410-004-0629-4.

Tormey, D. R., T. L. Grove, and W. B. Bryan (1987), Experimental petrology of normal MORB near the Kane Fracture Zone: 22°–25°N, mid-Atlantic ridge, *Contrib. Mineral. Petrol.*, *96*, 121–139, doi:10.1007/BF00375227.

Ulmer, P. (1989), The dependence of the Fe2+-Mg cation partitioning between olivine and basaltic liquid on pressure, temperature and composition: An experimental study on 30 kbars, *Contrib. Mineral. Petrol.*, *101*, 261–273, doi:10.1007/BF00375311.

Villiger, S., P. Ulmer, O. Müntener, and A. B. Thompson (2004), The liquid line of descent of anhydrous, mantle-derived, tholeiitic liquids by fractional and equilibrium crystallization: An experimental study at 1.0 GPa, *J. Petrol.*, *45*, 2369–2388, doi:10.1093/petrology/egh042.

Wagner, T. P., and T. L. Grove (1998), Melt/harzburgite reaction in the petrogenesis of tholeiitic magma from Kilauea volcano, Hawaii, *Contrib. Mineral. Petrol.*, *131*, 1–12, doi:10.1007/s004100050374.

Walker, D., T. Shibata, and E. DeLong (1979), Abyssal tholeiites from the Oceanographer Fracture Zone, *Contrib. Mineral. Petrol.*, *70*, 111–125, doi:10.1007/BF00374440.

Walter, M. J. (1998), Melting of garnet peridotite and the origin of komatiite and depleted lithosphere, *J. Petrol.*, *39*, 29–60, doi:10.1093/petroj/39.1.29.

Walter, M. J., and D. C. Presnall (1994), Melting behavior of simplified lherzolite in the system CaO-MgO-Al2O3-SiO2-Na2O from 7 to 35 kbar, *J. Petrol.*, *35*, 329–359.

Wasylenki, L. E., M. B. Baker, A. J. R. Kent, and E. M. Stolper (2003), Near-solidus melting of the shallow upper mantle: Partial melting experiments on depleted peridotite, *J. Petrol.*, *44*, 1163–1191, doi:10.1093/petrology/44.7.1163.

Workman, R. K., S. R. Hart, M. Jackson, M. Regelous, K. A. Farley, J. Blusztajn, M. Kurz, and H. Staudigel (2004), Recycled metasomatized lithosphere as the origin of the Enriched Mantle II (EM2) end-member: Evidence from the Samoan Volcanic Chain, *Geochem. Geophys. Geosyst.*, *5*, Q04008, doi:10.1029/2003GC000623.

Yang, H. J., R. J. Kinzler, and T. L. Grove (1996), Experiments and models of anhydrous, basaltic olivine-plagioclase-augite saturated melts from 0.001 to 10 kbar, *Contrib. Mineral. Petrol.*, *124*, 1–18, doi:10.1007/s004100050169.